Published in final edited form as:
Sci Signal. ; 9(443): ra86. doi:10.1126/scisignal.aaf3596.

Distinct microenvironmental cues stimulate divergent TLR4-mediated signaling pathways in macrophages

Anna M. Piccinini[*], **Lorena Zuliani-Alvarez**, **Jenny M. P. Lim**, and **Kim S. Midwood**[†]
Kennedy Institute of Rheumatology, Nuffield Department of Orthopaedics, Rheumatology and Musculoskeletal Sciences, University of Oxford, Headington, Oxford OX3 7FY, U.K.

Abstract

Macrophages exhibit a phenotypic plasticity that enables them to orchestrate specific immune responses to distinct threats. The microbial product lipopolysaccharide (LPS) and the extracellular matrix glycoprotein tenascin-C are released during bacterial infection and tissue injury, respectively, and both activate Toll-like receptor 4 (TLR4). We found that these two TLR4 ligands stimulated distinct signaling pathways in macrophages, resulting in cells with divergent phenotypes. Although macrophages activated by LPS or tenascin-C displayed some common features, including activation of nuclear factor κB and mitogen-activated protein kinase signaling and cytokine synthesis, each ligand stimulated the production of different subsets of cytokines and generated different phosphoproteomic signatures. Moreover, tenascin-C promoted the generation of macrophages that exhibited increased synthesis and phosphorylation of extracellular matrix components, whereas LPS stimulated the production of macrophages that exhibited an enhanced capacity to degrade the matrix. These data reveal how the activation of one pattern recognition receptor by different microenvironmental cues generates macrophage with distinct phenotypes.

Introduction

Macrophages are innate immune sentinels that patrol most tissues in the body. These cells detect changes in the microenvironment, including pathogen invasion and tissue damage, and mediate inflammatory processes, in response, that destroy microbial interlopers, remove and repair damaged tissue, and restore homeostasis (1). Macrophages are versatile cells that orchestrate both the induction and the resolution of inflammation. They can be driven toward a proinflammatory phenotype or a tissue repair phenotype by specific differentiation protocols in vitro. However, a much larger spectrum of macrophage subsets exists in vivo, enabling a context-dependent response to specific types and locations of threat (2). The microenvironment of these cells is therefore key to defining their behavior; both the surrounding cocktail of soluble cues (including cytokines, growth factors, and microbial

[†]Corresponding author. kim.midwood@kennedy.ox.ac.uk.
[*]Present address: School of Pharmacy, University of Nottingham, Nottingham NG7 2RD, U.K.

Author contributions: A.M.P., L.Z., and J.M.P.L. performed the experiments. A.M.P. and K.S.M. designed the experiments, analyzed the data, and wrote the paper.

Competing interests: The authors declare that they have no competing interests.

Data and materials availability: MS data from this study have been deposited in the PeptideAtlas repository with the identifier PASS00922.

Europe PMC Funders Author Manuscripts

products) and the network of extracellular matrix molecules specific to the tissue location of the macrophage affect its function (3, 4). Accumulating evidence demonstrates how environmental factors, including heme (5), retinoic acid (6), and transforming growth factor–β (TGF-β) (7), influence the specialization of tissue-resident macrophages. Moreover, studies of the transfer of tissue-resident macrophages to a different tissue showed that the microenvironment can reprogram fully differentiated macrophages (4).

Macrophages have pattern recognition receptors (PRRs), including Toll-like receptors (TLRs), nucleotide-binding oligomerization domain (NOD)–like receptors, retinoic acid–inducible gene 1 family members, lectins, and scavenger receptors, which they use to sense changes in the microenvironment (8). PRRs detect various threats; although receptor specificity exists, there is also a surprising amount of overlap in ligand recognition. For example, TLRs recognize pathogen-derived molecules, ranging from bacterial lipoproteins to viral nucleic acids, as well as endogenous molecules generated upon tissue damage, including self nucleic acids, phospholipids, small organic molecules, fatty acids, and various proteins and proteoglycans (9). This convergence of distinct microenvironmental signals on the same receptor family has raised the question of whether infection and sterile tissue injury are interpreted equivalently by the innate immune system. Although the mechanisms of pathogen-mediated TLR activation, signaling, and downstream inflammatory responses have been extensively investigated, those mediated by cues that indicate sterile tissue damage remain enigmatic.

We sought to undertake a systematic analysis of the signaling pathways and biological outcomes induced by two different stimuli, from infected and damaged microenvironments, respectively, that activate the same PRR. We directly compared two TLR4 activators: the Gram-negative bacterial lipopolysaccharide (LPS) and tenascin-C, an extracellular matrix glycoprotein that is produced specifically upon tissue injury (10). The activation of TLR4 by tenascin-C stimulates cytokine synthesis in various cells, including macrophages and fibroblasts (11–13). Although it is transiently produced upon tissue damage, tenascin-C is persistently found in chronic inflammatory diseases and in tumors (10). We previously demonstrated that the C-terminal fibrinogen-like globe (FBG) domain of tenascin-C is responsible for TLR4 activation and that this domain is potently arthritogenic, driving persistent TLR4-mediated disease in models of inflammatory arthritis (11). Here, we showed that activation of TLR4 by LPS or FBG generated macrophages with two distinct phenotypes, which displayed different activation markers, secreted different effector molecules, and induced different phosphoproteomic profiles underlying distinct signaling pathways and protein-protein interaction networks and generating macrophages with distinct catabolic and anabolic abilities. Together, our data provide evidence that the innate immune system can interpret the context of an inflammatory cue and orchestrate inflammation accordingly by instructing macrophage behavior.

Results

LPS and the FBG domain of tenascin-C stimulate distinct macrophage activation phenotypes

LPS recognition by TLR4 induces a well-defined macrophage phenotype (2). To determine whether the activation of TLR4 by FBG promotes a macrophage phenotype similar to that induced by LPS, we compared a combination of markers in LPS- and FBG-treated macrophages. We used human peripheral blood monocyte–derived macrophages cultured in macrophage colony-stimulating factor (M-CSF-MDMs) and examined macrophage markers that are increased in abundance by LPS or by alternative stimuli, such as interleukin-4 (IL-4) (14). Stimulation with either LPS (1 ng/ml) or 1 μM FBG domain induced comparable IL-6 secretion and *arginase-1* (*Arg1*) mRNA expression (Fig. 1A), whereas IL-23 and IL-12 secretion was induced only by LPS (Fig. 1B). At these concentrations of stimuli, FBG induced statistically significantly more IL-8 production (Fig. 1C) and less tumor necrosis factor–α (TNF-α) and IL-10 production (Fig. 1D) than did LPS. Finally, 1 μM FBG sustained the expression of the gene encoding mannose receptor, C type 1 (MRC1), whereas LPS (1 ng/ml) inhibited *MRC1* mRNA synthesis by 24 hours (Fig. 1E).

To rule out any contribution of contaminating LPS in FBG-stimulated macrophages, we pretreated FBG with polymyxin B, which neutralized LPS-induced cytokine synthesis but not that induced by FBG (fig. S1A). To ensure that differences in cell surface marker abundance were not due to the loss of viable cells upon stimulation, we assessed cytotoxicity with an MTT assay and found that neither LPS nor FBG had any effect on cell viability (fig. S1B). Finally, to confirm that the analyzed markers were directly increased in abundance in response to TLR4 activation, we stimulated macrophages with FBG or LPS in the presence or absence of an antibody that blocks TLR4 function or of TAK-242, an inhibitor of TLR4 signal transduction. Both TLR4 inhibitors effectively abrogated LPS- and FBG-induced cytokine synthesis (Fig. 1F) and reestablished basal *MRC1* expression (Fig. 1G). Together, these results suggest that macrophages recognize FBG and LPS through TLR4 and, in response, change their activation state toward alternatively [M(IL-4)] and classically [M(LPS)] (14) activated phenotypes, respectively.

LPS and the FBG domain of tenascin-C generate distinct macrophage phosphoproteomic signatures

To further examine differences between LPS- and FBG-activated macrophages, we assessed protein phosphorylation as readout of signal transduction in response to cell stimulation. Fluorescent two-dimensional difference gel electrophoresis (2D-DIGE) followed by mass spectrometry (MS) analysis was used to enable an unbiased and quantitative analysis of the global macrophage phosphoproteome (Fig. 2, A and B) (15). Macrophages were left unstimulated or were stimulated with LPS or the FBG domain of tenascin-C, and then immobilized metal ion affinity chromatography (IMAC) was used to enrich phosphorylated proteins from macrophage lysates. Yields of enriched phosphoprotein were quantified (fig. S2A), and the efficiency of phosphoprotein enrichment was verified (fig. S2, B to D). Phosphoproteins from control and LPS- and FBG-treated cells were each labeled with the fluorescent dye Cy3, whereas an internal standard, containing a mixture of equal amounts of

each experimental protein sample, was labeled with Cy5. Paired samples were separated by 2D polyacrylamide gel electrophoresis (2D-PAGE). Gels were subjected to multiwavelength fluorescent scanning to identify spots with at least 1.5-fold differences in intensity ($P \leq 0.05$) compared to the internal standard, and these spots were excised from a preparative gel for MS analysis. Sixty-eight phosphoproteins that were differentially regulated in abundance by stimulation with LPS or FBG compared to control cells were identified. LPS and FBG led to the differential regulation of 43 and 23 phosphoproteins, respectively, compared to control. Only two phosphoproteins, dermcidin isoform 2 (DCD-2) and prelamin-A/C (LMNA isoform Q5TCI8), were identified as being regulated by both stimuli (Fig. 2, C and D).

A number of proteins were selected for validation by Western blotting analysis of phosphoprotein fractions from control and LPS- and FBG-stimulated cells. These data confirmed the changes in abundance revealed by 2D-DIGE for proteasome subunit α6 (PSMA6), proteasome activator subunit 1 (PSME1), DCD, and type 1 collagen (COL1), as well as α-tubulin, which was included as a control because its abundance was not regulated by any stimulus (fig. S2E). Whereas Western blotting analysis confirmed the FBG-dependent increase in p38α [mitogen-activated protein kinase 14 (MAPK14)] phosphorylation that was observed by 2D-DIGE, it also showed that LPS stimulated the phosphorylation of p38α (fig. S2E). This signaling event was not identified in the proteomic screen but would be expected to occur based on what is known about the activation of TLR4 by LPS. Together, these data indicated that we could use the 2D-DIGE approach to identify subsets of signaling molecules activated by macrophages in response to different stimuli but do highlight that this technique will not yield an exhaustive list of all activated molecules. These data also emphasize the importance of independent validation to confirm data from this type of analysis, particularly when using primary human cells.

LPS- and FBG-stimulated protein phosphorylation drives divergent signaling pathways

To obtain insight into the types of proteins and the biological pathways in macrophages that were identified by 2D-DIGE as being regulated by LPS or FBG, we performed a number of in silico analyses. Gene ontology (GO) analysis examines the cellular location of regulated phosphoproteins, their class identity based on function and cellular compartment, and the biological systems to which they contribute. These data revealed that most of the macrophage phosphoproteins regulated by stimulation with LPS were intracellular, as expected (16), whereas there was an overrepresentation of extracellular phosphoproteins enriched from cells treated with FBG (fig. S3A). Chaperone, defense and immunity, and calcium-binding proteins were among the most highly populated classes of LPS-regulated phosphoproteins (fig. S3B). Accordingly, metabolic and immunological processes were well represented among the pathways associated with LPS-regulated phosphoproteins (fig. S3C). These observations are consistent with previous studies that investigated LPS-regulated protein phosphorylation in macrophages (16, 17). FBG-stimulated cells had distinct enriched protein classes, including extracellular matrix proteins, kinases, nucleic acid–binding proteins, receptor transporters, and surfactants, which were not observed in LPS-treated cells, and FBG-regulated phosphoproteins were also associated with distinct biological processes, such as apoptosis (fig. S3, B and C). However, LPS and FBG led to the enrichment of many common biological processes (for example, immune system processes,

cellular processes, and cellular component organization) and protein classes (for example, defense and immunity proteins, cytoskeletal proteins, transcription factors, enzyme modulators, transfer or carrier proteins, and proteases), indicating overlap in the biological outcomes that occur after the activation of macrophage TLR4 by each stimulus.

Next, we used the STRING (Search Tool for the Retrieval of Interacting Genes) database of known and predicted protein-protein interactions to identify specific pathways targeted by the phosphorylation events induced by LPS or FBG and to better understand the molecular organization and the relationships among these phosphoproteins. We first identified the top 15 statistically significantly enriched pathways downstream of LPS and FBG (Fig. 3, A and B). We next identified LPS-activated pathways that would be expected based on published data. These include MAPK signaling pathways (16, 17); endocytosis (16); immune signaling pathways, such as antigen processing and presentation (18), as well as complement (19) and coagulation (20) cascades; and infection-related pathways (for example, influenza A and Epstein-Barr virus infection), which corroborate a role for TLR4 signaling in response to viral infection (21). We also found representation of signaling pathways that substantiate emerging observations linking TLR signaling with endoplasmic reticulum activity in macrophages (22), estrogen signaling (23), spliceosome (24), thyroid hormone synthesis (25), and the biosynthesis of amino acids (26) (Fig. 3A). In contrast, distinct signaling pathways emerged from the analysis of FBG-stimulated cells. Consistent with the published literature, we observed enrichment for platelet activation (27), extracellular matrix–receptor interactions (28), focal adhesions (28, 29), leukocyte migration (30), phosphatidylinositol 3-kinase (PI3K)–Akt signaling (31), and vascular endothelial growth factor (VEGF) signaling (32) pathways. However, we also found distinct signaling pathways in immune defense, including amoebiasis, Epstein-Barr virus infection, NOD-like receptor signaling, shigellosis, and epithelial cell signaling in *Helicobacter pylori* infection. Furthermore, this analysis showed that FBG stimulation led to the phosphorylation of proteins associated with the proteasome.

We then analyzed the protein-protein interaction networks composed of phosphoproteins that were increased in abundance in response to LPS (1 ng/ml) and FBG (1 μM) (Fig. 3, C and D). We noted that 69% of LPS-responsive and 73% of FBG-responsive phosphoproteins were directly interconnected with each other in the STRING network. This high degree of connectivity suggests that LPS and FBG regulate components of functional pathways or protein complexes, rather than cause random protein phosphorylation events in macrophages. Furthermore, upon FBG stimulation of macrophages, this analysis predicted that MAPK11 (p38β) and MAPK14 (p38α or p38 MAPK) would act as central kinases and that collagen types I, II, and III would act as preponderant extracellular matrix molecules (Fig. 3D).

Together, these bioinformatics data highlight the biological outcomes that were common in response to LPS and the FBG domain of tenascin-C, but also reveal differences in the macrophage response to these distinct microenvironmental stimuli. However, although GO, KEGG (Kyoto Encyclopedia of Genes and Genomes) pathway, and protein interaction network analyses help to explore experimental data sets and provide testable hypotheses, independent experimental validation is required to draw any conclusions. We chose two

pathways to investigate further. The first was the MAPK signaling pathway, given that FBG-mediated phosphorylation of p38 kinases has not yet been investigated in macrophages, whereas the second was the phosphorylation of collagen molecules, given that this was particular to stimulation by FBG and, to our knowledge, has not been reported in macrophages.

Both LPS and the FBG domain of tenascin-C stimulate p38, c-Jun N-terminal kinase, and nuclear factor κB signaling through TLR4 activation

LPS-mediated activation of TLR4 stimulates the phosphorylation (and activation) of the MAPKs p38 and c-Jun N-terminal kinase (JNK) and the activation of nuclear factor κB (NF-κB)–dependent gene transcription. Phosphorylation of p38α and p38β emerged as a key event after the activation of macrophages of FBG (Fig. 4A and fig. S4A); however, little is known about MAPK signaling downstream of this TLR4 stimulus.

Western blotting analysis of phosphoprotein-enriched and unphosphorylated protein fractions from FBG-stimulated macrophages with an antibody specific for phosphorylated p38α (pp38α; Thr^{180}/Tyr^{182}) confirmed the activation of p38α by FBG (figs. S2E and S4B). We next compared the LPS- and FBG-stimulated phosphorylation of p38α over time in experiments with macrophage donors, independent of those used in the phosphoproteomic screen. Western blotting analysis of macrophage lysates for phosphoproteins revealed that both FBG and LPS stimulated p38α phosphorylation. Whereas p38α phosphorylation induced by FBG appeared to be more transient (maximal by 30 min in macrophages from all donors), that induced by LPS was sustained for longer times (Fig. 4B). FBG increased the extent of intracellular staining of pp38α (fig. S4C) and also stimulated the phosphorylation of MAPK kinase kinase 3 (MKK3) and MKK6, specific upstream kinases that are necessary for p38α activation (fig. S4D). Stimulation of cells with FBG or LPS also induced JNK phosphorylation; however, the magnitude of activation of JNK1 and JNK2/3 was greater in cells treated with LPS than in cells treated with FBG (Fig. 4C). In addition, FBG stimulated the degradation of a substantial amount of inhibitor of NF-κB α (IκBα), with maximal degradation at 90 min (30 min later than in the case of LPS) (Fig. 4D); however, it activated an NF-κB–driven reporter gene overexpressed in monocytic cell lines to a similar extent and with similar kinetics to that of LPS (fig. S4E). FBG-dependent MAPK and NF-κB activities were inhibited by the TLR4 function–blocking antibody (Fig. 4, E to G, and fig. S4F). These results suggest that, similarly to LPS, the FBG domain of tenascin-C stimulates the p38, JNK, and NF-κB pathways through the activation of TLR4.

The FBG domain of tenascin-C stimulates macrophages to synthesize and phosphorylate collagen

Among the phosphoproteins that increased the most in abundance in FBG-activated macrophages were collagen types I (*COL1A1* and *COL1A2*), II (*COL2A1*), and III (*COL3A1*). These molecules were not phosphorylated in either unstimulated or LPS-stimulated macrophages (Figs. 2B and 3D). We confirmed these data by subjecting phosphoprotein-enriched cellular fractions to Western blotting analysis with a collagen type I–specific antibody (fig. S2G). Although collagen phosphorylation was reported previously (33–38) [Cell Signaling Technology curation sets (www.PhosphoSitePlus.org)] (Fig. 5A),

the effect of collagen phosphorylation on its structure and function is unclear, and the biosynthesis of these large fibrillar extracellular matrix molecules by macrophages is not well characterized.

We examined whether the changes in the abundances of the collagens observed in our phosphoproteomic screen were regulated at the mRNA level after macrophage activation with LPS (1 ng/ml) or 1 μM FBG. *COL1A1* and *COL1A2* mRNA abundances in macrophages were similar in response to either LPS or FBG. In contrast, *COL2A1* mRNA was increased in abundance by FBG, but not by LPS, whereas *COL3A1* mRNA was undetectable (Fig. 5B). This stimulus-specific collagen production by macrophages was mediated through activation of TLR4 because the synthesis of *COL1A1, COL1A2*, and *COL2A1* mRNAs was prevented by TAK-242 (Fig. 5C). We extended this analysis to examine the expression of the genes encoding each of the 28 types of collagen in macrophages upon stimulation with LPS or FBG and compared the abundance of each collagen mRNA in macrophages with that in primary human dermal fibroblasts (DFs), one of the most prolific cellular sources of collagen. *COL10A1*, *COL11A1*, *COL16A1,* and *COL26A1* mRNAs were detected only in DFs, whereas *COL20A1* and *COL22A1* were not detected in either macrophages or DFs. With the exception of *COL17A1* mRNA, which was equally abundant in DFs and macrophages, and *COL23A1*, which was more abundant in macrophages than in DFs, macrophages had reduced amounts of collagen mRNAs compared to those in DFs, as expected (Fig. 5D and fig. S5E). The expression of *COL4A2*, *COL6A1*, *COL9A1*, *COL13A1*, *COL17A1*, *COL18A1*, *COL25A1,* and *COL27A1* in macrophages was regulated to a similar extent by both LPS and FBG. Compared to LPS, FBG was a stronger inducer of *COL8A1* expression, which is increased upon injury (39), and of *COL23A1* and *COL24A1*, which are found in cancer (40, 41), conditions in which tenascin-C plays an established role (42). In contrast to FBG, LPS induced increased expression of fibril-associated collagens with interrupted triple helices (FACITs), namely, *COL7A1*, *COL12A1*, *COL15A1*, *COL19A1*, and *COL21A1*, as well as the collagenase-resistant *COL5A1* and the collagen-containing von Willebrand factor *COL28A1* (Fig. 5D and fig. S5F). Together, these data show that macrophages can substantially contribute to collagen synthesis and that pathogenic stimuli drive the synthesis of FACIT collagens that maintain the integrity of the extracellular matrix, whereas matrix-derived cues instruct macrophages to synthesize *COL2A1* and phosphorylate collagens.

LPS, but not FBG, stimulates the synthesis of macrophage collagenases

To determine whether the degradation, as well as the synthesis, of collagen by macrophages was differentially affected by the FBG domain of tenascin-C and LPS, we investigated key matrix metalloproteinases (MMPs), including MMP1 (also known as interstitial collagenase), MMP13 (also known as collagenase 3), and MMP14, a type I transmembrane MMP that breaks down collagen, gelatin, and other matrix molecules. MMP1 abundance was statistically significantly and rapidly increased in response to LPS (1 ng/ml), whereas FBG (1 μM) resulted in a modest increase in MMP1 abundance at later time points. At this concentration, FBG did not stimulate MMP13 synthesis, which was in contrast to LPS, which promptly and transiently increased MMP13 abundance. Furthermore, MMP14 synthesis was induced 24 hours after stimulation with FBG, but not LPS (Fig. 6A). This

stimulus-specific MMP profile was mediated through the activation of TLR4 because the synthesis of each enzyme was completely abrogated by TAK-242 (Fig. 6B).

MMP activity is highly regulated at several levels. To determine whether the distinct expression of MMPs induced by the two TLR4 ligands resulted in functional differences, we tested the collagenolytic and gelatinolytic activities of LPS- and FBG-activated macrophages. LPS-activated macrophages efficiently degraded collagen, an activity that was reversed by the broad-spectrum MMP inhibitor GM6001, whereas FBG-activated cells showed little collagenolytic activity (Fig. 6C). These results are consistent with the collagenase expression profiles of each stimulus (*MMP1* mRNA and protein in Fig. 6A and fig. S6; *MMP13* mRNA in Fig. 6A). Macrophages constitutively degraded gelatin and continued to do so upon stimulation with FBG. Conversely, LPS-activated macrophages were unable to degrade gelatin (Fig. 6D, upper three panels). The gelatinolytic activity of macrophages did not match the changes in *MMP14* mRNA abundance (Fig. 6A), but did correlate with the cell surface abundance of MMP14 protein, which was low to undetectable in LPS-activated macrophages but largely unaltered in FBG-activated cells (Fig. 6D, lower panel), suggesting some degree of posttranscriptional regulation of MMP14 activity. Together, these data indicate that LPS, but not the FBG domain of tenascin-C, enables macrophages to degrade collagen but prevents them from degrading gelatin, thus affecting their substrate specificity.

Discussion

Detection of both pathogen invasion and sterile tissue damage by the same PRRs has been recognized for over a decade; however, the specificity of the inflammatory outcomes downstream of infection and injury remains poorly understood. This study directly compared the molecular signatures induced in primary human macrophages through activation of the same TLR by distinct microenvironmental stimuli. We showed that the proinflammatory, extracellular matrix glycoprotein tenascin-C and microbial LPS activated a common set of signaling pathways, including NF-κB and MAPK, but these stimuli also induced different signaling pathways downstream of TLR4. Although both stimuli resulted in cytokine synthesis, they differed in the cytokines that were produced. Moreover, the FBG domain of tenascin-C promoted a macrophage phenotype that exhibited matrix molecule synthesis and phosphorylation, whereas LPS promoted a macrophage phenotype characterized by an enhanced capacity to degrade matrix. Together, these data illustrate how the activation of TLR4 by ligands from endogenous (host-derived) and exogenous (microbe-derived) sources generates different macrophage phenotypes (Fig. 7).

Using a combination of markers of activation, we found two distinct activation phenotypes for macrophages that were exposed to either the FBG domain of tenascin-C or LPS. These data indicated that tenascin-C shifted the macrophage activation phenotype toward that induced by IL-4. Although FBG was unable to induce IL-12 or IL-23 production and induced less TNF-α production than did LPS, it sustained the expression of *MRC1*. The genes encoding IL-6 and Arg1, which are expressed throughout macrophage activation, were equally induced by both stimuli (14). However, although there was some overlap in the phenotypes generated by both stimuli, tenascin-C generated a type of macrophage that, in

contrast to IL-4–stimulated macrophages, resulted in less IL-10 production than occurred in response to LPS. These data exemplify the diverse nature of macrophage subsets, revealing how the microenvironment is key to fine-tuning their phenotypes.

By combining phosphoprotein enrichment with 2D-DIGE and MS analysis, we captured a snapshot of tenascin-C– and LPS-induced changes in the macrophage phosphoproteome that reflected the first 30 min of receptor activation. We also used multiple bioinformatics tools to explore the experimental data set. Although there are a few phosphoproteomic analyses of the responses of different TLRs to pathogenic ligands (16, 17), here, we compared the phosphoprotein signatures in response to stimulation of a specific TLR by exogenous and endogenous ligands. Overall, this analysis revealed two distinct yet overlapping phosphoproteomes. Consistent with this finding, Western blotting analysis confirmed that, whereas tenascin-C, and not LPS, stimulated PSMA6 phosphorylation and PSME1 dephosphorylation, both tenascin-C and LPS stimulated DCD phosphorylation. Bioinformatics analysis identified most of the LPS-dependent phosphoproteins as being intracellular and most of the tenascin-C–dependent proteins as being extracellular. The latter consisted of several extracellular matrix molecules, including COL1, which we validated by Western blotting, suggesting a role for the tenascin-C–mediated activation of TLR4 in changing the macrophage microenvironment. Along these lines, the KEGG pathway analysis and protein-protein interaction networks highlighted both differences and similarities among LPS- and tenascin-C–regulated phosphoproteins. On one hand, tenascin-C resulted in the enrichment of pathways that underlie an interplay between the cells and the microenvironment, including extracellular matrix–receptor interactions, focal adhesions, and leukocyte migration. Consistent with this, strong connectivity between matrix molecules emerged from the tenascin-C–dependent phosphoprotein interaction network. On the other hand, we observed an overlap in the innate immunity– and infection-related pathways that were activated by both stimuli.

As with other TLR phosphoproteomic studies (16, 17, 36), our study did not identify all of the phosphoproteins that belong to the TLR pathway, indicating that the screen does not completely recapitulate the complex effect of TLR activation in macrophages. Observational proteomic data sets are incomplete by nature because of either limited coverage of the regulated phosphoproteome or the possibility that not all pathway components are regulated by phosphorylation or have already been dephosphorylated or degraded at the time point chosen. However, the following findings strengthen the validity of our experimental data. First, we identified several phosphoproteins that are classically linked to the TLR pathway, including NF-κB [that is, NF-κB essential modulator (43) and clusterin (44)] and MAPK (that is, MAPK14 and MAPK11). Second, we detected the phosphorylation of cytoskeletal and actin-binding proteins, such as plastin-2 (45), septin-2, septin-11 (46), and vimentin (47), which are essential for macrophage motility and phagocytosis, as previously reported for LPS (16, 17). Third, we identified pathways that are linked to tenascin-C function, such as VEGF signaling (48) and focal adhesions (29). Fourth, we found phosphoproteins that are implicated in TLR activity [for example, annexin A1, annexin A2 (49, 50), and SWAP70 (51)] or are implicated in having a function for TLRs in glycolysis (52), such as α-enolase 1 and glyceraldehyde-3-phosphate dehydrogenase. Fifth, we identified kinases that are activated upon TLR4 activation, such as phosphatidylinositol-5-phosphate 4-kinase type 2α

(53–55) and eukaryotic elongation factor 2 kinase (56). Finally, we showed the enrichment of endogenous danger signals whose expression is induced upon TLR4 activation and can themselves activate TLR4 if released (57), such as S100A8, fibrinogen (FGB), and several heat shock proteins, including HSP90AB1, HSPA8, HSPA5, HSPA1L, and HSPA1A.

Independent experiments to validate tenascin-C–regulated phosphoproteins and targeted Western blotting analyses confirmed the activation of p38α MAPK and revealed the activation of JNK and NF-κB signaling, pathways that were also activated by LPS. Moreover, MS analysis revealed that in addition to Thr^{180} and Tyr^{182} (residues of p38α that are phosphorylated in response to LPS), phosphorylation of the previously uncharacterized residue Ser^{272} was induced by FBG. This event may be FBG-specific and could account, at least in part, for the differences in FBG- and LPS-stimulated signaling. However, we could not validate the phosphorylation of Ser^{272} in cells because a phosphospecific antibody for this site was not available.

We found that stimulation of macrophages with tenascin-C (1 μM), but not LPS (1 ng/ml), resulted in the enrichment of phosphorylated collagen. These data suggest that tenascin-C activates the synthesis and posttranslational modification of other matrix molecules by macrophages, and they place the production of phosphorylated collagen molecules in macrophages downstream of TLR signaling. Phosphorylation of extracellular matrix molecules, including collagen type I and secreted pro-α1(I) N-propeptide, by casein kinases was first reported more than 40 years ago (58, 59). More recently, phosphorylation of collagen type XVII was shown to inhibit its shedding by TNF-α converting enzyme TACE (34), and phosphorylation of other extracellular molecules is implicated in the regulation of cell adhesion and susceptibility to proteolytic cleavage. Note that the ability of tenascin-C to regulate the phosphorylation of nonkinase proteins has been reported. Tenascin-C promotes autophosphorylation of platelet-derived growth factor receptor A, thereby enhancing its ability to cross-talk with $\alpha_V\beta_3$ integrin and, in turn, promoting the proliferation and migration of smooth muscle cells (60).

Hemocytes, the phagocytes of invertebrates, synthesize collagen type IV in the germline stem cell niche in *Drosophila* (61). In humans, a handful of studies have reported the synthesis of collagen molecules in macrophages and have suggested that these proteins may play a role in anchoring macrophages to the extracellular matrix and stabilizing atherosclerotic plaques in vivo (62–64). One study looked at collagen mRNA synthesis by monocytes and macrophages; however, it only reported whether expression was detected or not without providing any quantitative data (64). We therefore screened for the expression of all 28 collagen-encoding mRNAs, including those found by the proteomic study, in LPS- or tenascin-C–activated and unactivated macrophages and compared it to that of human DFs, which are established matrix producers. With the exception of collagen type XXIII, whose mRNA was more abundant in macrophages, the abundances of 21 of the 22 collagen-encoding mRNAs detected in macrophages were greater in fibroblasts as expected. Note, however, that expression of the gene encoding collagen type II was substantially induced by tenascin-C, but not LPS, through the activation of TLR4. This indicates that matrix-derived, but not pathogenic, microenvironmental cues can instruct macrophages to synthesize collagen type II and reveals different phenotypic signatures of macrophages activated by

distinct stimuli that operate through the same receptor. This change in the cellular microenvironment may affect the interaction between the macrophage and the surrounding extracellular matrix, given that collagen type II interacts with integrins and proteoglycans (65, 66). The increased production of collagen type II by macrophages in response to tenascin-C may be relevant in diseases, such as rheumatoid arthritis, in which, on one hand, tenascin-C abundance is increased and sustains inflammation through TLR4 (11) and, on the other hand, antibodies against native and citrullinated collagen type II are produced (67). In vivo, it is possible that the production and modification of collagen by tenascin-C–activated macrophages counterbalances the production of degradative enzymes by these cells. This is supported by our findings that, upon activation of TLR4 by LPS, macrophages produced more MMP1 than did those activated by the FBG domain and that, at these concentrations, only LPS-activated macrophages produced MMP13 and degraded collagen in vitro. Thus, whereas tenascin-C enables macrophages to shape the biochemistry of the matrix, LPS enables macrophages to degrade it.

A number of questions remain to be answered, foremost of which is why distinct gene expression profiles are generated by a matrix-derived micro-environmental cue and a pathogenic component, given that both activate NF-κB and MAPK signaling by stimulating TLR4. The answer may lie in the recruitment of distinct adaptor molecules early in the signaling cascade. This process may be regulated by receptor dimerization, which is essential for signaling by pathogenic components but may not be necessary for signaling by endogenous molecules. Alternatively, this process may be explained by the distinct co-receptor and accessory molecule requirements for pathogenic and endogenous ligands to activate TLR4. For example, LPS requires the co-receptors MD-2 and CD14 to activate TLR4, whereas tenascin-C does not (11). In addition, hyaluronan fragments use MD-2 and CD44, but not CD14, and induce patterns of gene expression that are distinct from that induced by LPS (68).

Another key question relates to how the FBG domain activates macrophage TLR4 in vivo. What are the physiologically relevant concentrations and form(s) of this region of tenascin-C? Note that this study assessed the response of macrophages to single (and different) concentration of LPS and of the FBG domain of tenascin-C at a single time point. Thus, we can only make conclusions about how cells respond under these restricted conditions. It is also difficult to know how the concentrations of the stimuli that we examined correspond to what a macrophage encounters in vivo. Although tissue concentrations of tenascin-C in the range of 0.37 to 1.2 μM have been reported (69, 70), the amounts of tenascin-C are likely to be dependent on the tissue location and context. Moreover, here, we focused on a direct comparison of LPS- and FBG-mediated TLR4 signaling. It is possible that during tissue injury, tenascin-C is degraded, releasing proteolytic fragments consisting of the FBG domain, which are free to activate TLR4 in isolation from the rest of the tenascin-C molecule. FBG-containing tenascin-C fragments have been found in gingival crevicular fluid from a subset of periodontitis patients (71). Alternatively, macrophages could encounter intact tenascin-C that may either be soluble or incorporated into the tissue matrix. We previously showed that full-length tenascin-C induces TLR4-mediated cytokine synthesis equally as well as the FBG domain does alone (11). However, it will be important to examine not only how the FBG domain signals when present with other domains of

tenascin-C, which may together synergistically affect macrophage activation, but also how it signals within the context of an insoluble 3D multicomponent extracellular matrix.

In conclusion, our data suggest that specific stimuli induce overlapping, yet distinct, biological outcomes upon activation of the same innate immune receptor. This study provides evidence that the innate immune system can interpret qualitatively different challenges and instruct inflammatory responses accordingly. It also highlights not only the fact that the microenvironment affects TLR function but also that TLR activation affects the microenvironment. Understanding how the cellular microenvironment regulates macrophage phenotype and behavior may help address how to manipulate inflammation in response to tissue injury and infection.

Materials and Methods

Cell culture and stimulation

Primary human monocytes isolated from peripheral blood (London Blood Bank) were differentiated into macrophages (M-CSF-MDMs) by culturing them in RPMI 1640 containing 5% (v/v) fetal bovine serum (FBS) (Gibco), penicillin/streptomycin (100 U/ml; PAA), and recombinant human M-CSF (100 ng/ml; PeproTech) for 5 days (72). Adherent cells were washed, replated in RPMI 1640 containing 3% (v/v) FBS (Gibco) and penicillin/streptomycin (100 U/ml; PAA) for 24 hours before stimulation with LPS (1 ng/ml) [from *Escherichia coli* serotype EH100(Ra), TLR-grade; Enzo Life Sciences] or 1 μM FBG for 5, 15, or 30 min or for 1, 2, 3, 4, 8, or 24 hours. Recombinant human FBG was synthesized and purified as previously described (11) and, where stated, was preincubated with polymyxin B (10 μg/ml; Sigma). Primary human DFs were isolated from full-thickness skin samples. Tissue samples were dissected into small pieces and digested in Dulbecco's modified Eagle's medium (DMEM) with 1% (v/v) penicillin/streptomycin, 5% (v/v) FBS (Gibco), type I collagenase (Worthington Biochemical Corporation), and deoxyribonuclease I (Roche Diagnostics) for up to 2 hours at 37°C. Cells were cultured in DMEM with 10% (v/v) FBS and 1% (v/v) penicillin/streptomycin. Cells up to passage two were used for experiments.

Inhibitors

M-CSF-MDMs were stimulated for 30 min or 1, 1.5, 2, or 24 hours with FBG or LPS in the presence or absence of DMSO, TAK-242 (3 μM; Invivogen), pAb-h TLR (1, 10, or 25 μg/ml; Invivogen), isotype control antibody (rat pAb control; 1, 10, or 25 μg/ml; Invivogen), or GM6001 (10 μM).

Cell viability

Cell viability was examined by MTT assay (Sigma-Aldrich), according to the manufacturer's instructions.

Enzyme-linked immunosorbent assay

Cell supernatants were analyzed with ELISA kits to quantify TNF-α, IL-6 and IL-8 (R&D Systems), IL-10 and IL-12 (BD Biosciences), and IL-23 (eBioscience), according to the

manufacturers' instructions. Absorbance was read on a spectrophotometric ELISA plate reader, and the data were analyzed with Ascent Software (Thermo Labsystems).

Secreted embryonic alkaline phosphatase NF-κB activity assay

THP1-XBlue cells stably expressing an NF-κB–inducible and activating protein 1–inducible secreted embryonic alkaline phosphatase (SEAP) reporter gene (Invivogen) were cultured in RPMI 1640 supplemented with 10% (v/v) FBS (Gibco), penicillin (100 U/ml) and streptomycin (100 U/ml) (PAA), Normocin (100 μg/ml; Invivogen), and blasticidine-*S*-hydrochloride (10 μg/ml; Sigma). To monitor the activation of NF-κB signaling, 1×10^5 cells were stimulated with 0.5 μM FBG or LPS (0.5 ng/ml) for 1, 4, 8, or 24 hours, and the amount of secreted SEAP was measured by mixing 20 μl of the culture medium with 180 μl of QUANTI-Blue detection medium (Invivogen) and incubated for 2 hours at 37°C. Absorbance was measured at 620 nm with a FLUOstar Omega microplate reader (BMG LABTECH).

Phosphoprotein enrichment and CyDye labeling

M-CSF-MDMs (8×10^6) were treated with medium alone or with medium containing either 1 μM FBG or LPS (1 ng/ml) for 30 min before IMAC (73) was performed with the PhosphoProtein Purification Kit (Qiagen). Phosphoprotein-enriched fractions (5 μg) were labeled with 6 nM Cy3, whereas an internal standard, containing a mixture of equal amounts of each experimental protein sample, was labeled with 6 nM Cy5 saturation fluorescent dye, according to the manufacturer's instructions (CyDye DIGE Fluor Labeling Kit for Scarce Samples, GE Healthcare) by the proteomic services at the Cambridge Centre for Proteomics (www.bio.cam. ac.uk/proteomics). Briefly, labeling was optimized by titrating the reducing agent tris-(2-carboxyethyl)phosphine hydrochloride (TCEP) and the Cy3 and Cy5 dyes. The molar ratio of TCEP/dye was kept at 1:2 (1.5 nM TCEP and 3 nM dye; 2 nM TCEP and 4 nM dye; 2.5 nM TCEP and 5 nM dye; 3 nM TCEP and 6 nM dye; and 4 nM TCEP and 8 nM dye). The internal standard was included on each gel within the experiment. Proteins were reduced with 3 nM TCEP for 1 hour at 37°C in the dark and labeled with 6 nM Cy3 or Cy5 for 30 min at 37°C in the dark. The labeling reaction was quenched with 2× sample buffer (7 M urea, 2 M thiourea, and 4% CHAPS) containing 2% Pharmalytes and 130 mM dithiothreitol (DTT). Rehydration buffer [7 M urea, 2 M thiourea, 4% CHAPS, 1% Pharmalyte, and 13 mM DTT (broad-range pH 3 to 10)] was added before the labeled phosphoproteins were subjected to isoelectric focusing.

Two-dimensional difference gel electrophoresis

2D-DIGE was performed by the proteomic services at the Cambridge Centre for Proteomics, as previously described (15). Briefly, nonlinear immobilized pH gradient strips (13 cm long) (pH 3 to 10) (GE Healthcare) were rehydrated with CyDye-labeled samples at 20°C for 10 hours at 20 V with the IPGphor II apparatus (GE Healthcare), according to the manufacturer's instructions. Isoelectric focusing was performed for a total of 40,000 V·hour at 20°C at 50 mA. Before SDS-PAGE was performed, the strips were equilibrated for 15 min in 100 mM tris (pH 8.8), 30% (v/v) glycerol, 6 M urea, 2% (w/v) SDS, and 0.5% (w/v) DTT on a rocking table. The strips were loaded onto a 13-cm (1 mm thick), 12% acrylamide gel (pH 8.5) with a 1-cm, 4% stacker gel (pH 6.8). The strips were overlaid with 1% agarose in

SDS running buffer containing 5 mg of bromophenol blue. The gels were run at 20 mA for 15 min and then at 40 mA at 20°C until the bromophenol blue dye front had run off the bottom of the gels. A 10× tris/glycine/SDS running buffer (Bio-Rad) was used. A total of 13 gels were run, including 12 analytical gels (10 μg of phosphoproteins/gel) representing four biological replicates and one preparative gel (170 μg of combined phosphoproteins in total).

Gel imaging and statistical analysis

After 2D-DIGE, CyDye-labeled proteins were visualized with Typhoon 9400 Imager (GE Healthcare) to generate overlaid, multichannel images for each gel. The Cy3 images were scanned with a 532-nm laser and a 580-nm band pass 30 (BP30) emission filter. Cy5 images were scanned with a 633-nm laser and a 670-nm BP30 emission filter. To ensure maximum pixel intensity for the two dyes (between 40,000 and 60,000 pixels), all gels were scanned at 100-μm pixel resolution, and the photomultiplier tube voltage was set to between 500 and 700 V. The scanned gel images were then transferred to the ImageQuant version 5.2 software package (GE Healthcare). After cropping, the images were exported to the DeCyder Batch Processor and Biological Variation Analysis module (DeCyder 2D version 5.2 Software, GE Healthcare) for statistical analysis, according to the manufacturer's recommendations. To compare protein spots across gels, a master image was picked from images of the internal standard. The statistical analysis of changes in protein abundance between different cell stimulations was performed by the DeCyder–Biological Variation Analysis version 5.2 module. Landmark spots were manually defined to improve the automated matching results. The preparative gel was scanned and matched with the master gel to assign the right correspondence for spot picking. Data were normalized for computing the fold changes in abundance. Protein spots with a statistically significant variation ($P \leq 0.05$), showing a difference in volume of 1.5-fold compared to the same spots from unstimulated cell samples, were considered to be differentially abundant and were analyzed by MS.

Protein identification by MS

The preparative gel was silver-stained for spot excision. The silver-stained image was scanned and spot-matched to the fluorescent images to ensure the accurate excision of proteins of interest. Gel spots were excised from the gels with a 10-ml pipette tip and were placed into a 96-well PCR plate. The gel spots were destained, reduced with DTT, and alkylated with iodoacetamide before being subjected to enzymatic digestion with sequencing grade trypsin (Promega) overnight at 37°C. After digestion, the reaction mixture was pipetted into a sample vial and loaded onto an autosampler for automated LC-MS/MS analysis. All LC-MS/MS experiments were performed with the nanoACQUITY UPLC System (Waters Corporation) and an LTQ Orbitrap Velos hybrid ion trap mass spectrometer (Thermo Fisher Scientific). Separation of peptides was performed by reversed-phase chromatography with a Waters reversed-phase nanocolumn (BEH C18; 75 μm in diameter × 250 mm, 1.7-μm particle size) at a flow rate of 300 nl/min. Peptides were initially loaded onto a precolumn (Waters UPLC Trap Symmetry C18; 180 μm in diameter × 20 mm, 5-μm particle size) from the nanoACQUITY sample manager with 0.1% formic acid for 3 min at a flow rate of 10 μl/min. After this period, the column valve was switched to enable the elution of peptides from the precolumn onto the analytical column. Solvent A was water with 0.1%

formic acid, and solvent B was acetonitrile with 0.1% formic acid. The linear gradient used was 5 to 40% solvent B over 60 min. The LC eluant was sprayed into the mass spectrometer by means of a New Objective nanospray source. All mass/charge ratio values of eluting ions were measured in the Orbitrap Velos mass analyzer, set at a resolution of 30,000. Data-dependent scans (top 20) were used to automatically isolate and generate fragment ions by collision-induced dissociation in the linear ion trap, resulting in the generation of MS/MS spectra. Ions with charge states of 2^+ and above were selected for fragmentation. After the run, the data were processed with Protein Discoverer (version 1.2, Thermo Fisher Scientific). Briefly, all of the MS/MS data were converted to mgf files, and these were submitted to the Mascot search algorithm (Matrix Science) and searched against the UniProt human database, using a fixed modification of carbamidomethyl, a variable modification of oxidation, and in specific cases, phosphorylation using a peptide tolerance of 20 ppm (MS) and 0.1 Da (MS/MS). Peptide identifications were accepted if they could be established at a probability greater than 95.0%.

Bioinformatics analysis

GO annotation enrichment analysis was performed with the PANTHER version 8.1 classification system (www.pantherdb.org) (74). The background data set for the analysis was the *H. sapiens* genome, and the binomial test ($P < 0.05$) was used for statistical overrepresentation. KEGG pathway enrichment and interaction network analyses were performed with STRING version 10.0 (http://string-db.org/) (75). The background data set for the analyses was the *H. sapiens* genome. Experimentally observed protein phosphorylation data mining was conducted with PhosphoSitePlus (www.phosphosite.org/homeAction.do) (76). Hierarchical clustering was performed with MultiExperiment Viewer version 4.9 (www.tm4.org).

Phosphoprotein gel staining

Pro-Q Diamond Phosphoprotein Gel Stain (Molecular Probes) was used to selectively stain phosphoproteins in SDS-PAGE gels, according to the manufacturer's instructions. Gels were visualized with FLA-5100 Fluorescent Image Analyzer (Fuji Photo Film Co.) using 532-nm excitation and 580-nm long pass emission filters. Gels were then stained with silver stain to detect total protein.

Western blotting analysis

Phosphoprotein-enriched fractions (eluate) and the flow-through after IMAC-based separation of macrophage proteins were resolved by SDS-PAGE and analyzed by Western blotting with rabbit antibodies against human phosphorylated extracellular signal–regulated kinases 1 and 2 (#4370), human pp38α (#9211), human phosphorylated MKK3/MKK6 (#12280), human MKK3 (#8535), human MKK6 (#8550, Cell Signaling Technology), mouse 4G10 Platinum anti-phosphotyrosine (#05-1050, Millipore), rabbit anti-human α-tubulin (ab6046), rabbit anti-human PSMA6 (ab97563), rabbit anti-human PSME1 (ab140501), rabbit anti-human HSPA6 (ab96754, Abcam), rabbit anti-human DCD (PA5-13677, Thermo Fisher Scientific), and rabbit anti-human COL1 (H-197, Santa Cruz Biotechnology) antibodies. Cell extracts were analyzed by Western blotting with goat anti-human actin (I-19, Santa Cruz Biotechnology) and rabbit anti-human pp38α (#9211, Cell

Signaling Technology). Conditioned medium from LPS- and FBG-stimulated M-CSF-MDMs was analyzed by Western blotting with mouse anti-human MMP1 antibody (ab25483, Abcam). For validation experiments, 5×10^5 M-CSF-MDMs from new donors were stimulated, and cell extracts were prepared in 60 μl of lysis buffer [1% NP-40, 150 mM NaCl, and 20 mM tris (pH 7.5)] containing 10 mM EDTA, 10 mM EGTA, 1 mM Na_3VO_4, 5 mM NaF, and a protease inhibitor cocktail. Extracts were separated on 10% SDS-PAGE gels, and proteins were transferred to nitrocellulose membrane. The membranes were blocked in 5% bovine serum albumin (BSA) in tris-buffered saline (TBS) containing 0.1% Tween 20 (TBST) and were sequentially incubated with antibodies recognizing human pJNK (p46/54; #9521), human pp38α (#9211), human p38α (#8690, Cell Signaling Technology), human IκBα (C-15), human α-tubulin (B-7), human actin (I-19, Santa Cruz Biotechnology), and human β-tubulin (ab6046, Abcam). Blots were stripped of antibody between analyses with ReBlot Plus Strong Antibody Stripping Solution (Merck Millipore) and blocked again in 5% BSA-TBST. Densitometric analysis of bands was performed with Phoretix 1D Software (Totallab), and the results are presented as relative band volumes.

Immunofluorescence

M-CSF-MDMs were plated on glass coverslips and stimulated with 1 μM FBG or LPS (1 ng/ml). Cells were then fixed with 4% (v/v) paraformaldehyde (PFA) in TBS for 15 min at 4°C and permeabilized with 0.1% (v/v) Triton X-100 in TBS for 15 min at room temperature. Cells were incubated with blocking solution [5% (v/v) goat serum and 3% (w/v) BSA in TBS] for 1 hour at room temperature, which was followed by incubation for 1 hour at room temperature with anti-pp38α antibody (#9211, Cell Signaling Technology) diluted in blocking solution. After the cells were washed four times with TBS, they were incubated for 1 hour at room temperature with Alexa Fluor 568–conjugated secondary anti-rabbit immunoglobulin G (IgG) (Molecular Probes) diluted in blocking solution, and the nuclei were stained with DAPI. After the cells were washed four times in TBS, they were mounted onto glass slides with ProLong Gold Antifade Reagent (Invitrogen). Controls that were stained in the absence of primary antibody were also included. Images were captured by fluorescence microscopy (Zeiss Axio ScopeA.1 light/fluorescent microscope and AxioCam HRc camera). Multichannel images were generated with ImageJ software (http://imagej.nih.gov/ij/).

RNA extraction, quantitative real-time PCR, and RT-PCR

Total RNA was extracted from M-CSF-MDMs (1.5×10^6) with RNeasy Mini Kit (Qiagen). Complementary DNA (cDNA) was synthesized from equivalent amounts of total RNA with the High-Capacity cDNA Reverse Transcription Kit using random primers (Applied Biosystems). Quantitative real-time PCR was performed in a ViiA 7 machine (Applied Biosystems) with TaqMan primer sets for human *COL1A1* (Hs00164004_m1), *COL1A2* (Hs00164099_m1), *COL2A1* (Hs00264051_m1), *COL3A1* (Hs00943809_m1), *COL4A2* (Hs01098873_m1), *COL5A1* (Hs00609133_m1), *COL6A1* (Hs01095585_m1), *COL7A1* (Hs00164310_m1), *COL8A1* (Hs00156669_m1), *COL9A1* (Hs00932129_m1), *COL10A1* (Hs00166657_m1), *COL11A1* (Hs01097664_m1), *COL12A1* (Hs00189184_m1), *COL13A1* (Hs01103879_m1), *COL14A1* (Hs00964045_m1), *COL15A1* (Hs01557124_m1), *COL16A1* (Hs00156876_m1), *COL17A1* (Hs00990036_m1),

COL18A1 (Hs00181017_m1), *COL19A1* (Hs00156940_m1), *COL20A1* (Hs00612130_m1), *COL21A1* (Hs00229402_m1), *COL22A1* (Hs01377192_m1), *COL23A1* (Hs00297526_m1), *COL24A1* (Hs00537698_m1), *COL25A1* (Hs00261300_m1), *COL26A1* (Hs00294957_m1), *COL27A1* (Hs00259829_m1), *COL28A1* (Hs00417144_m1), *MMP1* (Hs00899658_m1), *MMP13* (Hs00233992_m1), *MMP14* (Hs00237119_m1), *MRC1* (Hs00267207_m1), *Arg1* (Hs00968979_m1), and *HPRT1* (Hs02800695_m1). Changes in mRNA abundance in stimulated cells were calculated by the change-in-threshold ($\Delta\Delta C_T$) method with *HPRT1* as the endogenous control for gene expression and were normalized to results obtained from unstimulated cells.

Collagen film degradation assay

A collagen film degradation assay was performed as described previously (77). Briefly, M-CSF-MDMs were seeded on six-well culture plates coated with a thin layer of fibrillar type I bovine collagen (3 mg/ml; PureCol) in the presence or absence of LPS or FBG, and with or without GM6001. Five days later, the cells were removed by trypsinization, and the plates were fixed with 3% PFA in TBS for 20 min and stained with Coomassie Brilliant Blue R250. Images were captured with a charge-coupled device (CCD) camera–equipped microscope (Nikon TE2000-E). Degraded areas were visualized as white, unstained, and noncollagen-containing zones.

Fluorescently labeled gelatin film degradation assay

A gelatin film degradation assay was performed as described previously (77). Briefly, glass coverslips (18 mm in diameter) were coated with Alexa Fluor 488–conjugated gelatin. M-CSF-MDMs were seeded onto the fluorescently labeled gelatin–coated coverslips in the presence or absence of LPS or FBG, with or without GM6001, and were cultured for 64 hours. The cells were then fixed with 3% PFA in TBS for 15 min and immunostained. Cells were then incubated with blocking solution [5% (v/v) goat serum and 3% (w/v) BSA in TBS] for 1 hour at room temperature, which was followed by incubation for 2 hours at room temperature with rabbit anti-human MMP14 (ab51074, Abcam). After the cells were washed four times with TBS, they were incubated for 1 hour at room temperature with Alexa Fluor 568–conjugated secondary anti-rabbit IgG (Molecular Probes) diluted in blocking solution, and the nuclei were stained with DAPI. After the cells were washed four times with TBS, they were mounted onto glass slides with ProLong Gold Antifade Reagent (Invitrogen). Controls that were stained in the absence of primary antibody were included. Images were captured with a CCD camera–equipped microscope (Nikon TE2000-E). Degraded areas were visualized as dark, nonfluorescent zones.

Statistical analysis

Statistical analysis was performed with paired *t* test by one-way ANOVA, or by two-way ANOVA, with Sidak's multiple comparisons test, where appropriate, with Prism 6 software (GraphPad software).

Supplementary Materials

Refer to Web version on PubMed Central for supplementary material.

Acknowledgments

We thank Y. Shitomi and K. Yamamoto for advice on collagen and gelatin film degradation assays and MMP1 protein detection, S. Giblin for providing RNA extracted from human DFs, L. Thompson for critically reading the manuscript, and A. Judge for confirming our use of appropriate statistical analyses.

Funding: This work was supported by the Medical Research Council, Arthritis Research U.K., and the Kennedy Trust for Rheumatology Research.

References and Notes

1. Wynn TA, Chawla A, Pollard JW. Macrophage biology in development, homeostasis and disease. Nature. 2013; 496:445–455. [PubMed: 23619691]
2. Mosser DM, Edwards JP. Exploring the full spectrum of macrophage activation. Nat Rev Immunol. 2008; 8:958–969. [PubMed: 19029990]
3. Epelman S, Lavine KJ, Randolph GJ. Origin and functions of tissue macrophages. Immunity. 2014; 41:21–35. [PubMed: 25035951]
4. Lavin Y, Winter D, Blecher-Gonen R, David E, Keren-Shaul H, Merad M, Jung S, Amit I. Tissue-resident macrophage enhancer landscapes are shaped by the local microenvironment. Cell. 2014; 159:1312–1326. [PubMed: 25480296]
5. Haldar M, Kohyama M, So AY-L, KC W, Wu X, Briseño CG, Satpathy AT, Kretzer NM, Arase H, Rajasekaran NS, Wang L, et al. Heme-mediated SPI-C induction promotes monocyte differentiation into iron-recycling macrophages. Cell. 2014; 156:1223–1234. [PubMed: 24630724]
6. Okabe Y, Medzhitov R. Tissue-specific signals control reversible program of localization and functional polarization of macrophages. Cell. 2014; 157:832–844. [PubMed: 24792964]
7. Abutbul S, Shapiro J, Szaingurten-Solodkin I, Levy N, Carmy Y, Baron R, Jung S, Monsonego A. TGF-β signaling through SMAD2/3 induces the quiescent microglial phenotype within the CNS environment. Glia. 2012; 60:1160–1171. [PubMed: 22511296]
8. Taylor PR, Martinez-Pomares L, Stacey M, Lin H-H, Brown GD, Gordon S. Macrophage receptors and immune recognition. Annu Rev Immunol. 2005; 23:901–944. [PubMed: 15771589]
9. Bryant CE, Gay NJ, Heymans S, Sacre S, Schaefer L, Midwood KS. Advances in Toll-like receptor biology: Modes of activation by diverse stimuli. Crit Rev Biochem Mol Biol. 2015; 50:359–379. [PubMed: 25857820]
10. Udalova IA, Ruhmann M, Thomson SJP, Midwood KS. Expression and immune function of tenascin-C. Crit Rev Immunol. 2011; 31:115–145. [PubMed: 21542790]
11. Midwood K, Sacre S, Piccinini AM, Inglis J, Trebaul A, Chan E, Drexler S, Sofat N, Kashiwagi M, Orend G, Brennan F, et al. Tenascin-C is an endogenous activator of Toll-like receptor 4 that is essential for maintaining inflammation in arthritic joint disease. Nat Med. 2009; 15:774–780. [PubMed: 19561617]
12. Patel L, Sun W, Glasson SS, Morris EA, Flannery CR, Chockalingam PS. Tenascin-C induces inflammatory mediators and matrix degradation in osteoarthritic cartilage. BMC Musculoskelet Disord. 2011; 12:164. [PubMed: 21762512]
13. Kuriyama N, Duarte S, Hamada T, Busuttil RW, Coito AJ. Tenascin-C: A novel mediator of hepatic ischemia and reperfusion injury. Hepatology. 2011; 54:2125–2136. [PubMed: 21898491]
14. Murray PJ, Allen JE, Biswas SK, Fisher EA, Gilroy DW, Goerdt S, Gordon S, Hamilton JA, Ivashkiv LB, Lawrence T, Locati M, et al. Macrophage activation and polarization: Nomenclature and experimental guidelines. Immunity. 2014; 41:14–20. [PubMed: 25035950]
15. Lilley KS. Protein profiling using two-dimensional difference gel electrophoresis (2-D DIGE). Curr Protoc Protein Sci. 2003; 22:1–14. [PubMed: 18429242]
16. Weintz G, Olsen JV, Frühauf K, Niedzielska M, Amit I, Jantsch J, Mages J, Frech C, Dölken L, Mann M, Lang R. The phosphoproteome of toll-like receptor-activated macrophages. Mol Syst Biol. 2010; 6:371. [PubMed: 20531401]
17. Sjoelund V, Smelkinson M, Nita-Lazar A. Phosphoproteome profiling of the macrophage response to different toll-like receptor ligands identifies differences in global phosphorylation dynamics. J Proteome Res. 2014; 13:5185–5197. [PubMed: 24941444]

18. Blander JM. Coupling Toll-like receptor signaling with phagocytosis: Potentiation of antigen presentation. Trends Immunol. 2007; 28:19–25. [PubMed: 17126600]
19. Morrison DC, Kline LF. Activation of the classical and properdin pathways of complement by bacterial lipopolysaccharides (LPS). J Immunol. 1977; 118:362–368. [PubMed: 318670]
20. Koch L, Hofer S, Weigand MA, Frommhold D, Poeschl J, Ruef P. Inhibition of LPS-induced activation of coagulation by p38 MAPK inhibitor. ISRN Hematol. 2012; 2012:762614. [PubMed: 22461999]
21. Shirey KA, Lai W, Scott AJ, Lipsky M, Mistry P, Pletneva LM, Karp CL, McAlees J, Gioannini TL, Weiss J, Chen WH, et al. The TLR4 antagonist Eritoran protects mice from lethal influenza infection. Nature. 2013; 497:498–502. [PubMed: 23636320]
22. Goto Y, Ogawa K, Nakamura TJ, Hattori A, Tsujimoto M. TLR-mediated secretion of endoplasmic reticulum aminopeptidase 1 from macrophages. J Immunol. 2014; 192:4443–4452. [PubMed: 24688025]
23. Calippe B, Douin-Echinard V, Delpy L, Laffargue M, Lélu K, Krust A, Pipy B, Bayard F, Arnal J-F, Guery J-C, Gourdy P. 17β-estradiol promotes TLR4-triggered proinflammatory mediator production through direct estrogen receptor α signaling in macrophages in vivo. J Immunol. 2010; 185:1169–1176. [PubMed: 20554954]
24. Shashkin PN, Brown GT, Ghosh A, Marathe GK, McIntyre TM. Lipopolysaccharide is a direct agonist for platelet RNA splicing. J Immunol. 2008; 181:3495–3502. [PubMed: 18714022]
25. Yamazaki K, Suzuki K, Yamada E, Yamada T, Takeshita F, Matsumoto M, Mitsuhashi T, Obara T, Takano K, Sato K. Suppression of iodide uptake and thyroid hormone synthesis with stimulation of the type I interferon system by double-stranded ribonucleic acid in cultured human thyroid follicles. Endocrinology. 2007; 148:3226–3235. [PubMed: 17395700]
26. Galván-Peña S, O'Neill LAJ. Metabolic reprograming in macrophage polarization. Front Immunol. 2014; 5:420. [PubMed: 25228902]
27. Schaff M, Receveur N, Bourdon C, Wurtz V, Denis CV, Orend G, Gachet C, Lanza F, Mangin PH. Novel function of tenascin-C, a matrix protein relevant to atherosclerosis, in platelet recruitment and activation under flow. Arterioscler Thromb Vasc Biol. 2011; 31:117–124. [PubMed: 20651280]
28. Midwood KS, Hussenet T, Langlois B, Orend G. Advances in tenascin-C biology. Cell Mol Life Sci. 2011; 68:3175–3199. [PubMed: 21818551]
29. Ghert MA, Qi WN, Erickson HP, Block JA, Scully SP. Tenascin-C splice variant adhesive/anti-adhesive effects on chondrosarcoma cell attachment to fibronectin. Cell Struct Funct. 2001; 26:179–187. [PubMed: 11565810]
30. Clark RA, Erickson HP, Springer TA. Tenascin supports lymphocyte rolling. J Cell Biol. 1997; 137:755–765. [PubMed: 9151679]
31. Gong X-G, Lv Y-F, Li X-Q, Xu F-G, Ma Q-Y. Gemcitabine resistance induced by interaction between alternatively spliced segment of tenascin-C and annexin A2 in pancreatic cancer cells. Biol Pharm Bull. 2010; 33:1261–1267. [PubMed: 20686216]
32. Sumioka T, Fujita N, Kitano A, Okada Y, Saika S. Impaired angiogenic response in the cornea of mice lacking tenascin C. Invest Ophthalmol Vis Sci. 2011; 52:2462–2467. [PubMed: 21087965]
33. Urushizaki Y, Seifter S. Phosphorylation of hydroxylysine residues in collagen synthesized by cultured aortic smooth muscle cells. Proc Natl Acad Sci USA. 1985; 82:3091–3095. [PubMed: 3858806]
34. Zimina EP, Fritsch A, Schermer B, Bakulina AY, Bashkurov M, Benzing T, Bruckner-Tuderman L. Extracellular phosphorylation of collagen XVII by ecto-casein kinase 2 inhibits ectodomain shedding. J Biol Chem. 2007; 282:22737–22746. [PubMed: 17545155]
35. Olsen D, Jiang J, Chang R, Duffy R, Sakaguchi M, Leigh S, Lundgard R, Ju J, Buschman F, Truong-Le V, Pham B, et al. Expression and characterization of a low molecular weight recombinant human gelatin: Development of a substitute for animal-derived gelatin with superior features. Protein Expr Purif. 2005; 40:346–357. [PubMed: 15766877]
36. Sharma K, D'Souza RCJ, Tyanova S, Schaab C, Wisniewski JR, Cox J, Mann M. Ultradeep human phosphoproteome reveals a distinct regulatory nature of Tyr and Ser/Thr-based signaling. Cell Rep. 2014; 8:1583–1594. [PubMed: 25159151]

37. Beausoleil SA, Villén J, Gerber SA, Rush J, Gygi SP. A probability-based approach for high-throughput protein phosphorylation analysis and site localization. Nat Biotechnol. 2006; 24:1285–1292. [PubMed: 16964243]
38. Molina H, Horn DM, Tang N, Mathivanan S, Pandey A. Global proteomic profiling of phosphopeptides using electron transfer dissociation tandem mass spectrometry. Proc Natl Acad Sci USA. 2007; 104:2199–2204. [PubMed: 17287340]
39. Adiguzel E, Hou G, Mulholland D, Hopfer U, Fukai N, Olsen B, Bendeck M. Migration and growth are attenuated in vascular smooth muscle cells with type VIII collagen-null alleles. Arterioscler Thromb Vasc Biol. 2006; 26:56–61. [PubMed: 16269661]
40. Banyard J, Bao L, Zetter BR. Type XXIII collagen, a new transmembrane collagen identified in metastatic tumor cells. J Biol Chem. 2003; 278:20989–20994. [PubMed: 12644459]
41. Misawa K, Kanazawa T, Imai A, Endo S, Mochizuki D, Fukushima H, Misawa Y, Mineta H. Prognostic value of type XXII and XXIV collagen mRNA expression in head and neck cancer patients. Mol Clin Oncol. 2014; 2:285–291. [PubMed: 24649348]
42. Midwood KS, Orend G. The role of tenascin-C in tissue injury and tumorigenesis. J Cell Commun Signal. 2009; 3:287–310. [PubMed: 19838819]
43. Rothwarf DM, Zandi E, Natoli G, Karin M. IKK-γ is an essential regulatory subunit of the IκB kinase complex. Nature. 1998; 395:297–300. [PubMed: 9751060]
44. Bartuzi P, Hofker MH, van de Sluis B. Tuning NF-κB activity: A touch of COMMD proteins. Biochim Biophys Acta. 2013; 1832:2315–2321. [PubMed: 24080195]
45. Janji B, Giganti A, De Corte V, Catillon M, Bruyneel E, Lentz D, Plastino J, Gettemans J, Friederich E. Phosphorylation on Ser5 increases the F-actin-binding activity of L-plastin and promotes its targeting to sites of actin assembly in cells. J Cell Sci. 2006; 119:1947–1960. [PubMed: 16636079]
46. Mostowy S, Cossart P. Septins: The fourth component of the cytoskeleton. Nat Rev Mol Cell Biol. 2012; 13:183–194. [PubMed: 22314400]
47. Katsumoto T, Mitsushima A, Kurimura T. The role of the vimentin intermediate filaments in rat 3Y1 cells elucidated by immunoelectron microscopy and computer-graphic reconstruction. Biol Cell. 1990; 68:139–146. [PubMed: 2192768]
48. Tanaka K, Hiraiwa N, Hashimoto H, Yamazaki Y, Kusakabe M. Tenascin-C regulates angiogenesis in tumor through the regulation of vascular endothelial growth factor expression. Int J Cancer. 2004; 108:31–40. [PubMed: 14618612]
49. Bist P, Shu S, Lee H, Arora S, Nair S, Lim JY, Dayalan J, Gasser S, Biswas SK, Fairhurst A-M, Lim LHK. Annexin-A1 regulates TLR-mediated IFN-β production through an interaction with TANK-binding kinase 1. J Immunol. 2013; 191:4375–4382. [PubMed: 24048896]
50. Swisher JFA, Burton N, Bacot SM, Vogel SN, Feldman GM. Annexin A2 tetramer activates human and murine macrophages through TLR4. Blood. 2010; 115:549–558. [PubMed: 19965653]
51. Chopin M, Chacón-Martínez CA, Jessberger R. Fine tuning of IRF-4 expression by SWAP-70 controls the initiation of plasma cell development. Eur J Immunol. 2011; 41:3063–3074. [PubMed: 21728176]
52. Kelly B, O'Neill LAJ. Metabolic reprogramming in macrophages and dendritic cells in innate immunity. Cell Res. 2015; 25:771–784. [PubMed: 26045163]
53. Nguyen NTT, Kim YM, Kim TD, Le OTT, Kim JJ, Kang HC, Hasegawa H, Kanaho Y, Jou I, Lee SY. Phosphatidylinositol 4-phosphate 5-kinase a facilitates Toll-like receptor 4-mediated microglial inflammation through regulation of the Toll/interleukin-1 receptor domain-containing adaptor protein (TIRAP) location. J Biol Chem. 2013; 288:5645–5659. [PubMed: 23297396]
54. Le OT, Nguyen TT, Lee SY. Phosphoinositide turnover in Toll-like receptor signaling and trafficking. BMB Rep. 2014; 47:361–368. [PubMed: 24856829]
55. Chiang C-Y, Veckman V, Limmer K, David M. Phospholipase Cγ-2 and intracellular calcium are required for lipopolysaccharide-induced Toll-like receptor 4 (TLR4) endocytosis and interferon regulatory factor 3 (IRF3) activation. J Biol Chem. 2012; 287:3704–3709. [PubMed: 22158869]
56. Carpenter S, Ricci EP, Mercier BC, Moore MJ, Fitzgerald KA. Post-transcriptional regulation of gene expression in innate immunity. Nat Rev Immunol. 2014; 14:361–376. [PubMed: 24854588]

57. Piccinini AM, Midwood KS. DAMPening inflammation by modulating TLR signalling. Mediators Inflamm. 2010; 2010:672395. [PubMed: 20706656]
58. Veis A, Sfeir C, Wu CB. Phosphorylation of the proteins of the extracellular matrix of mineralized tissues by casein kinase-like activity. Crit Rev Oral Biol Med. 1997; 8:360–379. [PubMed: 9391750]
59. Volpin D, Veis A. Cyanogen bromide peptides from insoluble skin and dentin bovine collagens. Biochemistry. 1973; 12:1452–1464. [PubMed: 4348835]
60. Ishigaki T, Imanaka-Yoshida K, Shimojo N, Matsushima S, Taki W, Yoshida T. Tenascin-C enhances crosstalk signaling of integrin αvβ3/PDGFR-β complex by SRC recruitment promoting PDGF-induced proliferation and migration in smooth muscle cells. J Cell Physiol. 2011; 226:2617–2624. [PubMed: 21792920]
61. Van De Bor V, Zimniak G, Papone L, Cerezo D, Malbouyres M, Juan T, Ruggiero F, Noselli S. Companion blood cells control ovarian stem cell niche microenvironment and homeostasis. Cell Rep. 2015; 13:546–560. [PubMed: 26456819]
62. Vaage J, Lindblad WJ. Production of collagen type I by mouse peritoneal macrophages. J Leukoc Biol. 1990; 48:274–280. [PubMed: 2202772]
63. Weitkamp B, Cullen P, Plenz G, Robenek H, Rauterberg J. Human macrophages synthesize type VIII collagen in vitro and in the atherosclerotic plaque. FASEB J. 1999; 13:1445–1457. [PubMed: 10428768]
64. Schnoor M, Cullen P, Lorkowski J, Stolle K, Robenek H, Troyer D, Rauterberg J, Lorkowski S. Production of type VI collagen by human macrophages: A new dimension in macrophage functional heterogeneity. J Immunol. 2008; 180:5707–5719. [PubMed: 18390756]
65. Leitinger B, Hohenester E. Mammalian collagen receptors. Matrix Biol. 2007; 26:146–155. [PubMed: 17141492]
66. Scott JE. Extracellular matrix, supramolecular organisation and shape. J Anat. 1995; 187(Pt. 2): 259–269. [PubMed: 7591990]
67. Rowley MJ, Nandakumar KS, Holmdahl R. The role of collagen antibodies in mediating arthritis. Mod Rheumatol. 2008; 18:429–441. [PubMed: 18521704]
68. Taylor KR, Yamasaki K, Radek KA, Di Nardo A, Goodarzi H, Golenbock D, Beutler B, Gallo RL. Recognition of hyaluronan released in sterile injury involves a unique receptor complex dependent on Toll-like receptor 4, CD44, and MD-2. J Biol Chem. 2007; 282:18265–18275. [PubMed: 17400552]
69. Lightner VA, Slemp CA, Erickson HP. Localization and quantitation of hexabrachion (tenascin) in skin, embryonic brain, tumors, and plasma. Ann N Y Acad Sci. 1990; 580:260–275. [PubMed: 1692456]
70. Ventimiglia JB, Wikstrand CJ, Ostrowski LE, Bourdon MA, Lightner VA, Bigner DD. Tenascin expression in human glioma cell lines and normal tissues. J Neuroimmunol. 1992; 36:41–55. [PubMed: 1370958]
71. Ruggiero S, Cosgarea R, Potempa J, Potempa B, Eick S, Chiquet M. Cleavage of extracellular matrix in periodontitis: Gingipains differentially affect cell adhesion activities of fibronectin and tenascin-C. Biochim Biophys Acta. 2013; 1832:517–526. [PubMed: 23313574]
72. Goh FG, Piccinini AM, Krausgruber T, Udalova IA, Midwood KS. Transcriptional regulation of the endogenous danger signal tenascin-C: A novel autocrine loop in inflammation. J Immunol. 2010; 184:2655–2662. [PubMed: 20107185]
73. Machida M, Kosako H, Shirakabe K, Kobayashi M, Ushiyama M, Inagawa J, Hirano J, Nakano T, Bando Y, Nishida E, Hattori S. Purification of phosphoproteins by immobilized metal affinity chromatography and its application to phosphoproteome analysis. FEBS J. 2007; 274:1576–1587. [PubMed: 17480206]
74. Mi H, Muruganujan A, Casagrande JT, Thomas PD. Large-scale gene function analysis with the PANTHER classification system. Nat Protoc. 2013; 8:1551–1566. [PubMed: 23868073]
75. Szklarczyk D, Franceschini A, Wyder S, Forslund K, Heller D, Huerta-Cepas J, Simonovic M, Roth A, Santos A, Tsafou KP, Kuhn M, et al. STRING v10: Protein–protein interaction networks, integrated over the tree of life. Nucleic Acids Res. 2015; 43:D447–D452. [PubMed: 25352553]

76. Hombeck PV, Zhang B, Murray B, Komhauser JM, Latham V, Skrzypek E. PhosphoSitePlus, 2014: Mutations, PTMs and recalibrations. Nucleic Acids Res. 2015; 43:D512–D520. [PubMed: 25514926]

77. Woskowicz AM, Weaver SA, Shitomi Y, Ito N, Itoh Y. MT-LOOP-dependent localization of membrane type I matrix metalloproteinase (MT1-MMP) to the cell adhesion complexes promotes cancer cell invasion. J Biol Chem. 2013; 288:35126–35137. [PubMed: 24165131]

Europe PMC Funders Author Manuscripts

Europe PMC Funders Author Manuscripts

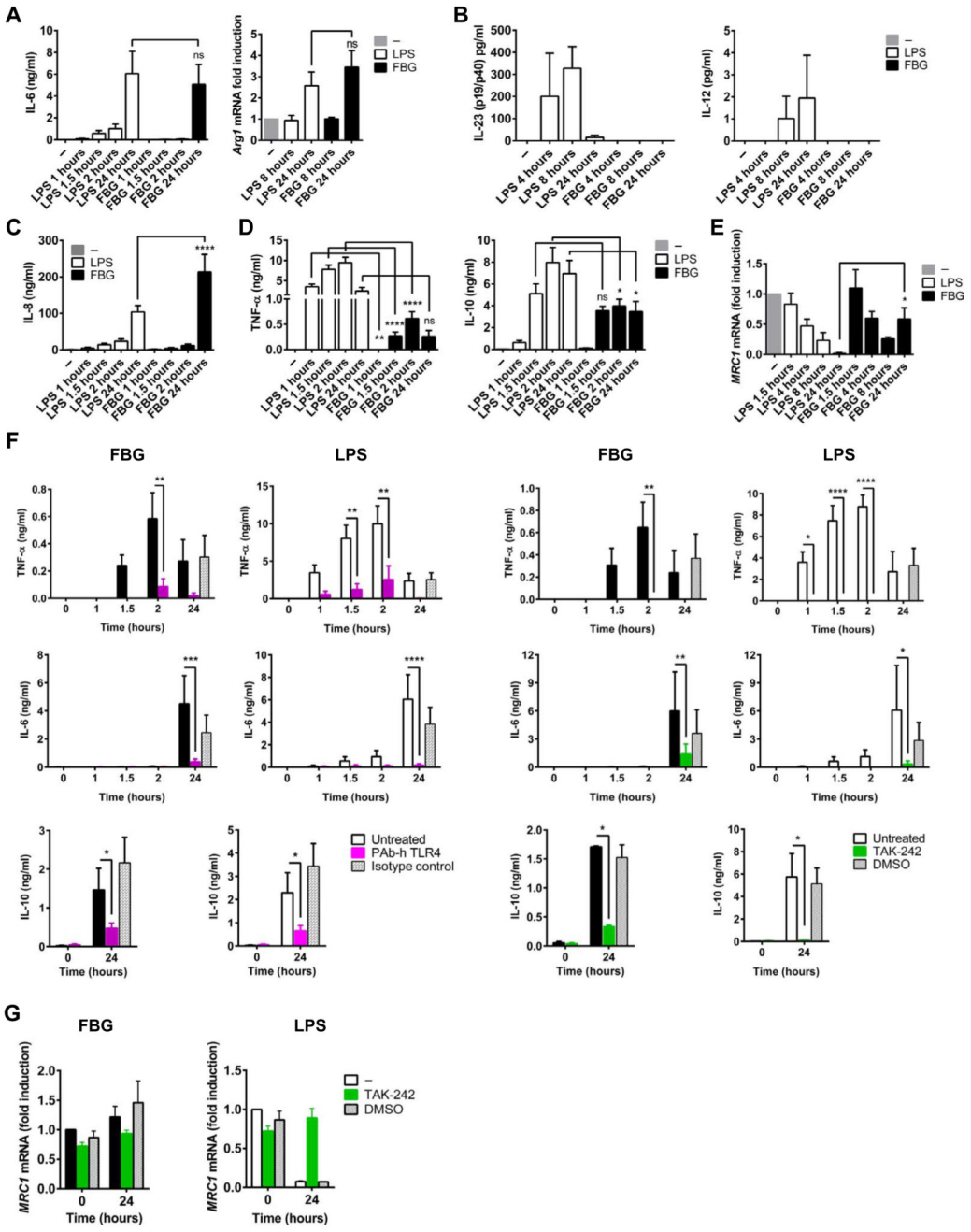

Fig. 1. Activation of M-CSF-MDMs upon stimulation of TLR4 with LPS or the FBG domain of tenascin-C.

(**A**) Left: M-CSF-MDMs were stimulated for the indicated times with LPS (1 ng/ml) or 1 μM FBG (preincubated with polymyxin B), and the amount of IL-6 secreted was determined by enzyme-linked immunosorbent assay (ELISA). Data are means ± SEM of nine independent experiments, each with a different donor. Right: Quantitative reverse transcription polymerase chain reaction (RT-qPCR) analysis of *Arg1* mRNA in M-CSF-MDMs stimulated for 8 or 24 hours with LPS or FBG. Results are presented relative to the

abundance of *Arg1* mRNA in unstimulated cells. Data are means ± SEM of four independent experiments, each with a different donor. ns, not significant by one-way analysis of variance (ANOVA). (**B to D**) M-CSF-MDMs were stimulated for the indicated times with LPS or FBG as described in (A) before the amounts of IL-23 and IL-12 (B), IL-8 (C), and TNF-α and IL-10 (D) secreted were determined by ELISA. Data are means ± SEM of five to nine independent experiments, each with a different donor. $*P < 0.05$, $**P < 0.01$, $****P < 0.0001$ by one-way ANOVA. (**E**) RT-qPCR analysis of *MRC1* mRNA in M-CSF-MDMs stimulated for the indicated times with LPS or FBG. Results are presented relative to the abundance of *MRC1* mRNA in unstimulated cells. Data are means ± SEM of four independent experiments, each with a different donor. $*P < 0.05$ by one-way ANOVA. (**F**) M-CSF-MDMs were stimulated for the indicated times with LPS or FBG in the presence or absence of polyclonal anti-human TLR4 antibody (pAb-h TLR4) or isotype control (left) or 3 μM TAK-242 or dimethyl sulfoxide (DMSO) (right). The amounts of TNF-α, IL-6, and IL-10 secreted were determined by ELISA. Data are means ± SEM of three to five (left) or three or four (right) independent experiments, each with a different donor. $*P < 0.05$, $**P < 0.01$, $***P < 0.001$, $****P < 0.0001$ by two-way ANOVA. (**G**) RT-qPCR analysis of *MRC1* mRNA in M-CSF-MDMs stimulated for 24 hours with LPS or FBG in the presence or absence of 3 μM TAK-242 or DMSO. Results are presented relative to the *MRC1* mRNA abundance of unstimulated cells. Data are means ± SEM of three independent experiments, each with a different donor.

Europe PMC Funders Author Manuscripts

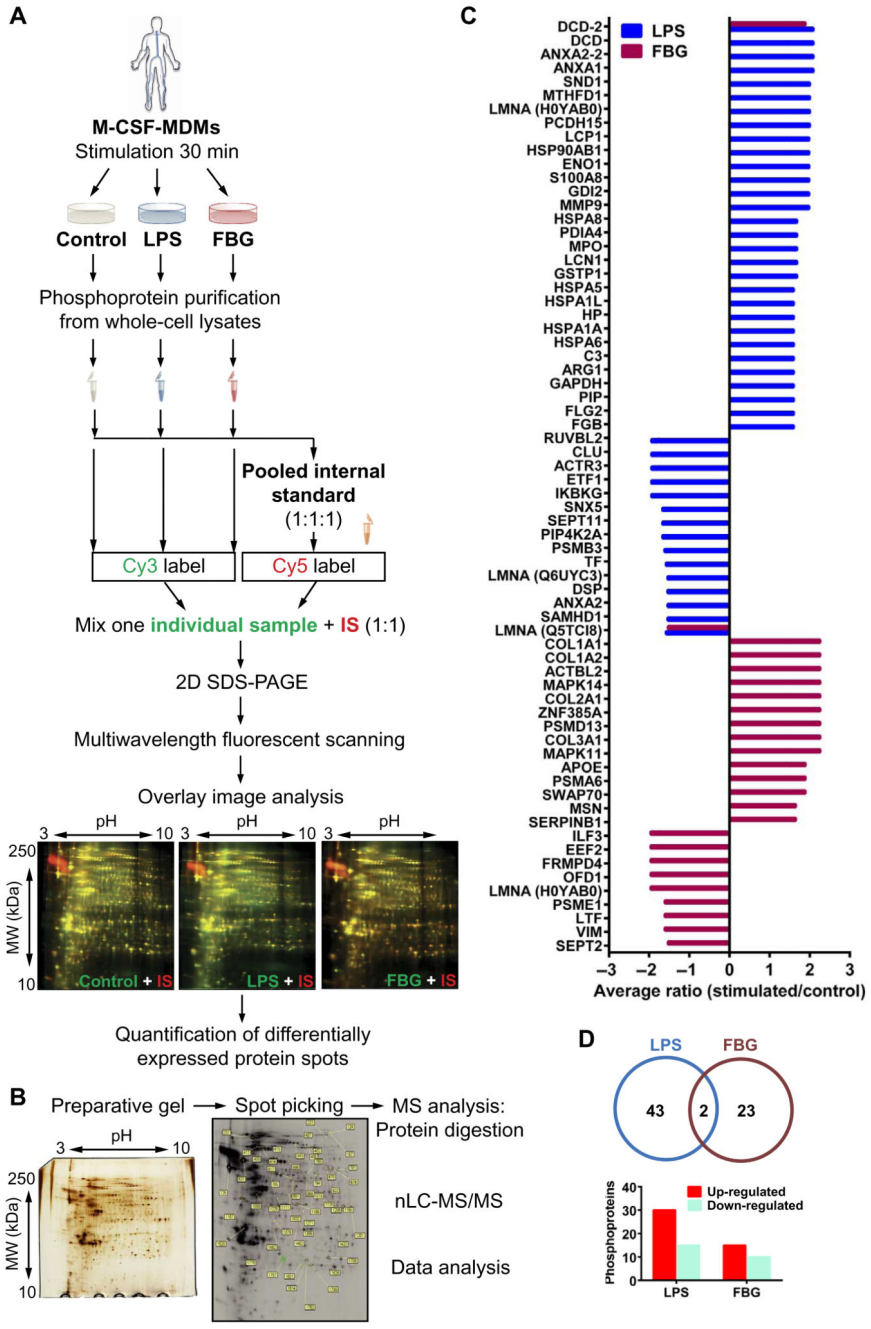

Fig. 2. Phosphoproteomic profiling of M-CSF-MDMs stimulated with LPS or FBG.

(**A**) Workflow of phosphoprotein enrichment and analysis in human M-CSF-MDMs by IMAC and 2D-DIGE. Cells were left unstimulated or were stimulated with LPS (1 ng/ml) or 1 μM FBG for 30 min, and cell lysates were then subjected to IMAC to enrich phosphoproteins. Four different donors were used for each condition. Phosphoprotein-enriched fractions from individual samples and the internal standard (IS; a pool of equal amounts of each biological replicate) were labeled with CyDye DIGE Fluor Cy3 (green) and Cy5 (red) saturation dyes, respectively, which was followed by 2D-DIGE. 2D analytical gels

Europe PMC Funders Author Manuscripts

were loaded with 5 μg of Cy3-labeled individual sample and 5 μg of Cy5-labeled IS. From each gel, two scanned images were generated at different wavelengths and overlaid. Differentially expressed protein spots were identified and quantified with DeCyder 2D Differential Analysis Software ($P < 0.05$, as determined by Student's t test; average ratio, ≥1.5). Representative 2D analytical gels (pH 3 to 10) from one donor. MW, molecular weight. (**B**) Workflow of protein identification from 2D-DIGE by MS analysis. Left: A preparative gel was loaded with 120 μg of total phosphoproteins [10 μg of each phosphoprotein-enriched fraction prepared from the lysates of cells treated as described in (A) and then subjected to silver staining]. This was matched to the analytical gel set with DeCyder 2D software to identify the differentially abundant protein spots that were determined by 2D-DIGE analysis. Right: The differentially abundant spots that were selected for automated spot picking before protein digestion, followed by nanoscale liquid chromatographic tandem mass spectrometry (nLC-MS/MS) analysis and Mascot database searching. (**C**) Phosphoproteins whose abundance was differentially regulated by LPS or FBG. Histogram shows increased and decreased abundance as an average ratio. This is the normalized ratio between LPS-stimulated cells and unstimulated cells and between FBG-stimulated cells and unstimulated cells. $n = 4$ independent donors per group. Phosphoproteins are shown with gene names. Data are from one experiment and are representative of four biological replicates. (**D**) Venn diagram displays phosphoproteins shared and specific to LPS- and FBG-stimulated M-CSF-MDMs. Histogram shows the numbers of phosphoproteins whose abundance was statistically significantly increased or decreased by LPS or FBG. Data are from one experiment and are representative of four biological replicates.

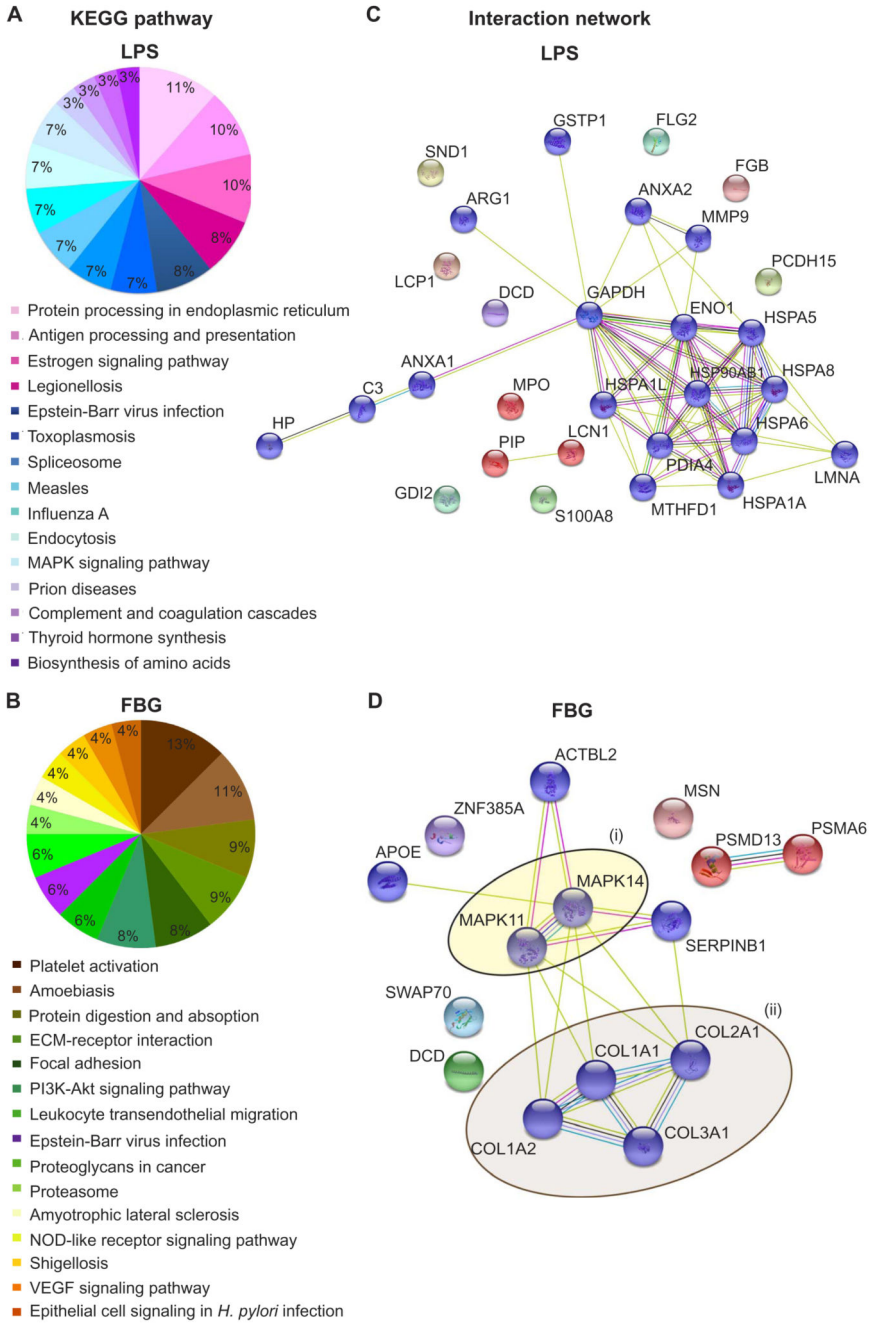

Fig. 3. Regulated pathways and protein networks in LPS-stimulated versus FBG-stimulated M-CSF-MDMs.

(**A** and **B**) Pathway analysis of phosphoproteins whose abundance in M-CSF-MDMs was statistically significantly increased by stimulation for 30 min with LPS (A) or the FBG domain of tenascin-C (B). Pie charts show the top 15 statistically significantly enriched KEGG pathways ($P < 0.05$) among the regulated phosphoproteins after LPS or FBG stimulation compared to those of unstimulated cells. For each KEGG pathway, pie chart slices show the percentage of gene hits against the total number of genes. KEGG pathway

enrichment was performed with STRING, and the background data set for the analysis was the *Homo sapiens* genome. ECM, extracellular matrix. (**C** and **D**) Interaction networks of phosphoproteins whose abundance in M-CSF-MDMs was statistically significantly increased by stimulation for 30 min with LPS (C) or FBG (D). The networks were constructed with STRING. Nodes (circles) represent phosphoproteins regulated by LPS (C) and FBG (D) and are labeled with gene names. Both connected and disconnected nodes are shown. Nodes were clustered and colored with the Markov Cluster algorithm according to their distance matrix. Edges (lines) indicate known and predicted protein-protein interactions and are drawn with differently colored lines according to the type of evidence: neighborhood (green), co-occurrence (dark blue), experimental (purple), text-mining (olive green), database (blue), homology (light blue), and coexpression (black). Ovals highlight proteins that belong to enriched KEGG pathways that were investigated here. Proteins in group (i) belong to the platelet activation, leukocyte transendothelial migration, Epstein-Barr virus infection, proteoglycans in cancer, amyotrophic lateral sclerosis, NOD-like receptor signaling, shigellosis, VEGF signaling, and epithelial cell signaling in *H. pylori* infection pathways. Proteins in group (ii) belong to the platelet activation, amoebiasis, protein digestion and absorption, extracellular matrix–receptor interaction, focal adhesion, and PI3K-Akt signaling pathways.

Europe PMC Funders Author Manuscripts

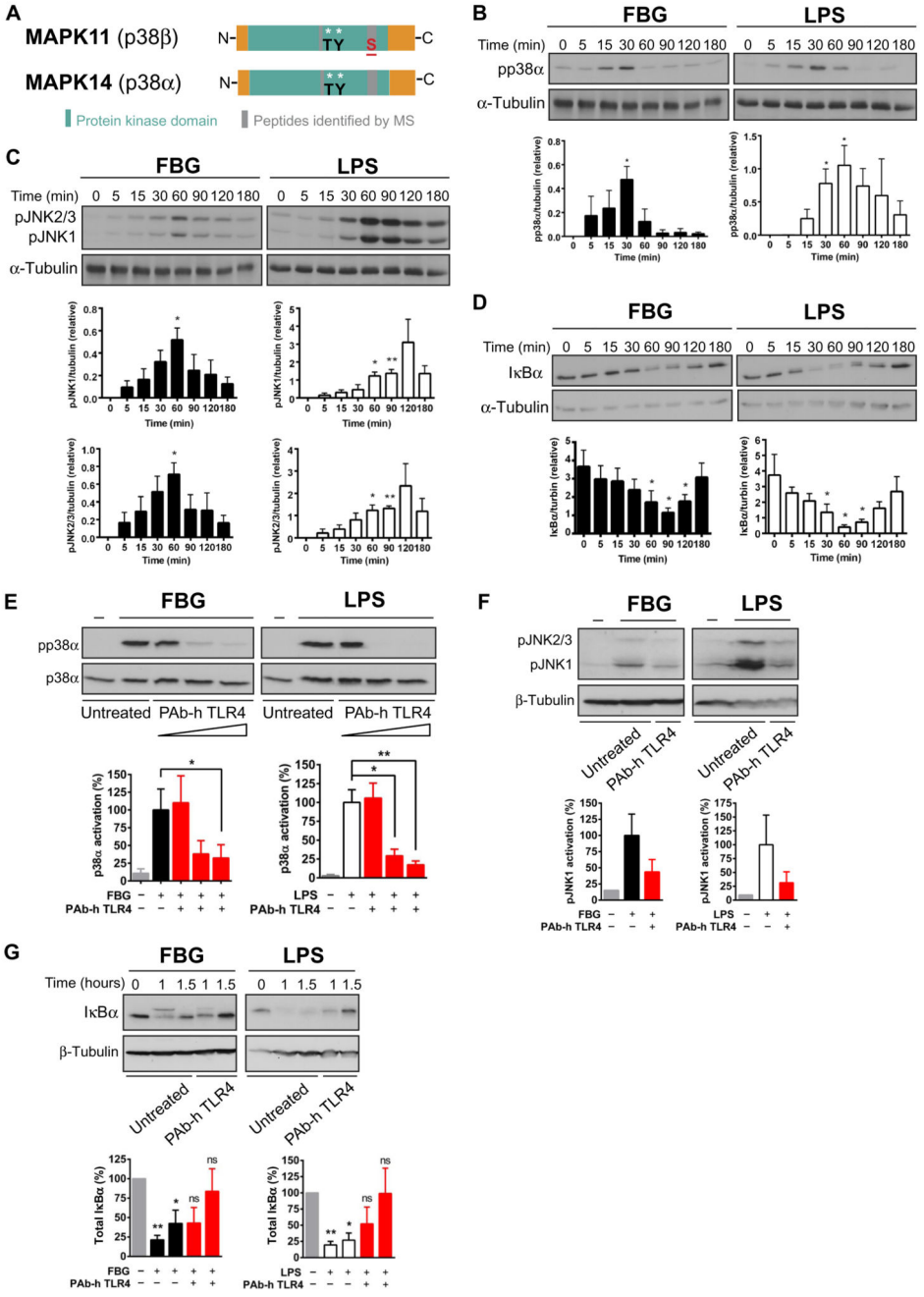

Fig. 4. The FBG domain of tenascin-C and LPS stimulate p38α, JNK, and NF-κB signaling through TLR4.

(**A**) Schematic representation of MAPK11 (p38β) and MAPK14 (p38α). The protein kinase domain is shown in green, and the flanking N- and C-terminal regions are in orange. Peptide sequences that were found by MS analysis are in gray. Starred black letters indicate published phosphorylation sites, whereas underlined red letters indicate the phosphorylation site identified in this study (Ser^{272}). (**B** to **D**) Top: M-CSF-MDMs were treated for the indicated times with 1 μM FBG or LPS (1 ng/ml), and cell lysates were then subjected to

Europe PMC Funders Author Manuscripts

Western blotting analysis with antibodies specific for pp38α (B), phosphorylated JNK1 (pJNK1) and pJNK2/3 (C), IκBα (D), and α-tubulin (B to D). Blots are representative of four independent experiments, each with a different donor. Bottom: Histograms show quantification of the abundances of pp38α (B), pJNK1 and pJNK2/3 (C), and IκBα (D) normalized to that of α-tubulin by densitometric analysis. Data are means ± SEM of four experiments. $*P < 0.05$, $**P < 0.01$ compared to the 0-min time point by one-way ANOVA. (**E** to **G**) Top: M-CSF-MDMs were treated for 30 min (E), 1 hour (F), or 1 and 1.5 hours (G) with 1 μM FBG or LPS (1 ng/ml) in the presence or absence of pAb-h TLR4 at dosages 1, 10, or 25 μg/ml (E) or 25 μg/ml (F and G). Cell lysates were then analyzed by Western blotting with antibodies specific for pp38α and total p38α (E), pJNK2/3 and pJNK1 (F), IκBα (G), and β-tubulin (F and G). Blots are representative of three or four independent experiments, each with a different donor. Bottom: Histograms show quantification of the abundances of pp38α (E), pJNK1 (F), and IκBα (G) normalized to the abundances of total p38 (E) and β-tubulin (F and G) by densitometric analysis. Data are expressed as a percentage of the abundance of the indicated proteins in cells stimulated in the absence of pAb-h TLR4. Data are means ± SEM of three or four independent experiments, each with a different donor. $*P < 0.05$, $**P < 0.01$. ns, not significant by one-way ANOVA.

Europe PMC Funders Author Manuscripts

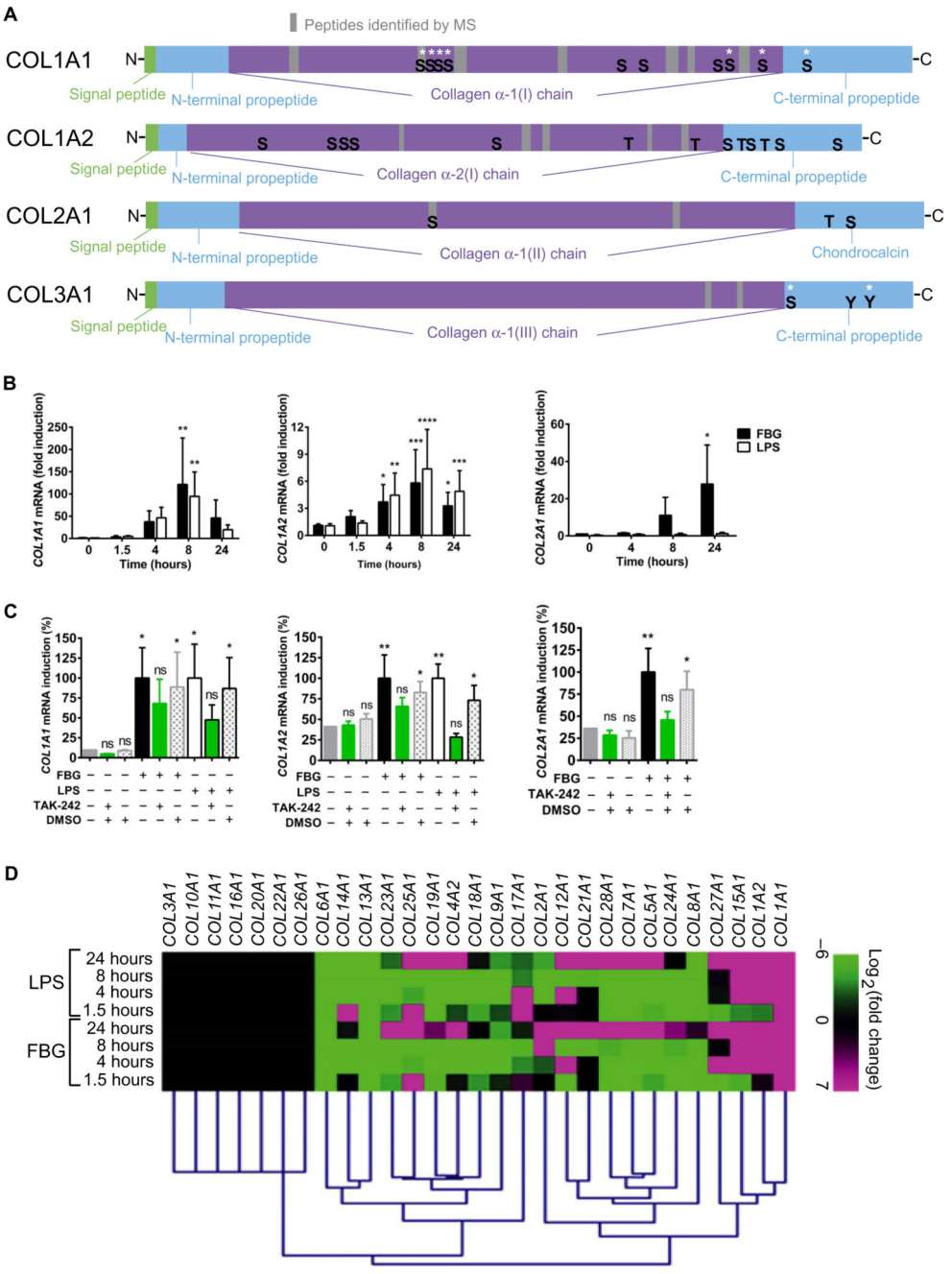

Fig. 5. Analysis of the collagen network in FBG- and LPS-activated M-CSF-MDMs.

(**A**) Schematic representation of COL1A1, COL1A2, COL2A1, and COL3A1. Green, signal peptide sequences; blue, N- and C-terminal propeptide sequences; purple, collagen chain sequences; gray, peptide sequences that were found by MS analysis. Letters indicate unpublished phosphorylation sites experimentally observed by Cell Signaling Technology [PhosphoSitePlus (www.phosphosite.org/homeAction.do)], and starred letters indicate published phosphorylation sites. (**B**) M-CSF-MDMs were stimulated for the indicated times with 1 μM FBG or LPS (1 ng/ml) and then were subjected to RT-qPCR analysis of the

Europe PMC Funders Author Manuscripts

abundances of *COL1A1*, *COL1A2*, and *COL2A1* mRNAs, which are expressed relative to their abundances in unstimulated cells. Data are means ± SEM of three to five independent experiments, each with a different donor. *$P < 0.05$, **$P < 0.01$, ***$P < 0.001$, ****$P < 0.0001$ by two-way ANOVA. (**C**) RT-qPCR analysis of *COL1A1*, *COL1A2*, and *COL2A1* mRNAs in M-CSF-MDMs stimulated with FBG or LPS for 8 (*COL1A1* and *COL1A2*) or 24 hours (*COL2A1*) in the presence or absence of 3 μM TAK-242 or DMSO control. Data are means ± SEM of four or five independent experiments, each with a different donor, and are presented as the percentage increase in mRNA abundance relative to that in cells stimulated in the absence of TAK-242 or DMSO. *$P < 0.05$, **$P < 0.01$ by one-way ANOVA when comparing stimulated to unstimulated cells. (**D**) RT-qPCR analysis of the abundances of the indicated collagen-encoding mRNAs in M-CSF-MDMs stimulated with FBG or LPS for the indicated times. The heat map shows suppression (green) and induction (magenta) of expression as fold change in mRNA abundance on a $\log_2$ scale relative to that in unstimulated cells. Connecting lines represent hierarchical clustering of the patterns of variation in expression of collagen-encoding genes. Data are from three independent experiments, each with a different donor.

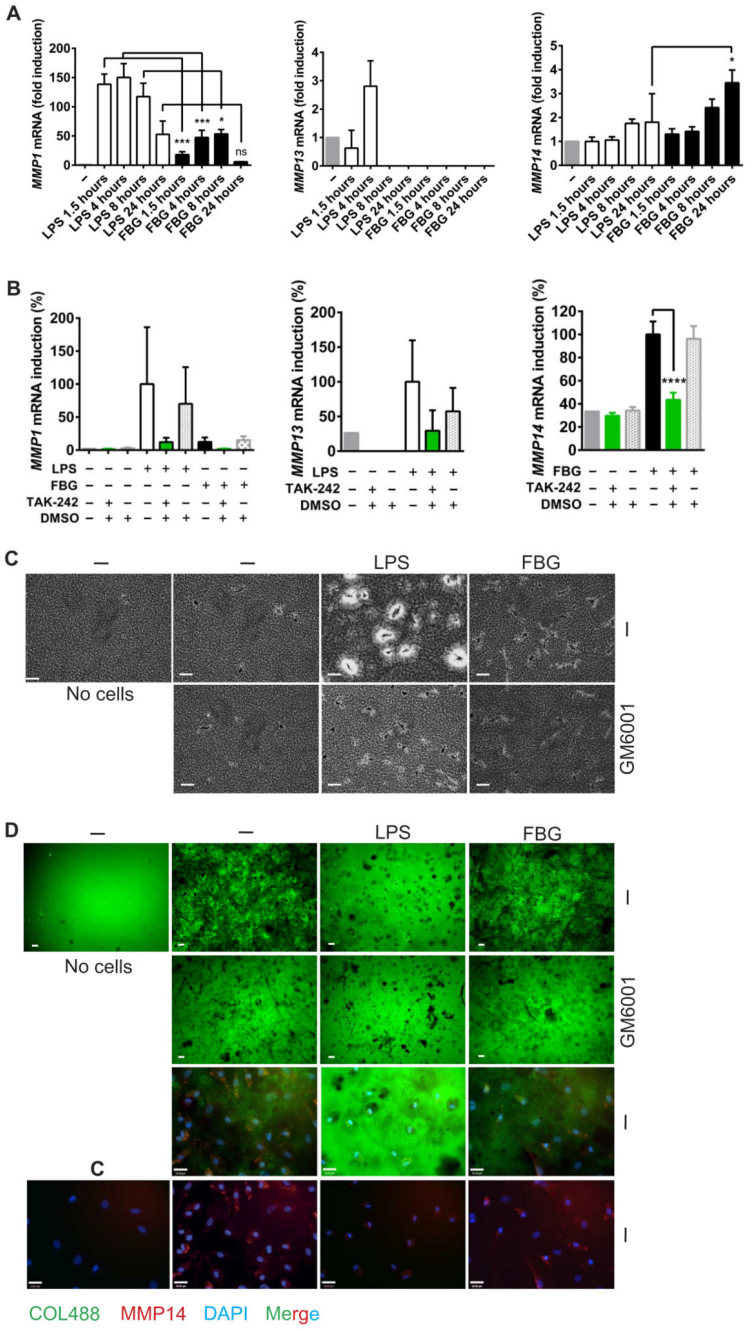

Fig. 6. MMP mRNA expression and matrix degradation by FBG- and LPS-activated M-CSF-MDMs.

(**A**) RT-qPCR analysis of *MMP1*, *MMP13*, and *MMP14* mRNA abundances in M-CSF-MDMs stimulated with LPS (1 ng/ml) or 1 μM FBG for the indicated times and expressed as a percentage of the mRNA abundances of unstimulated cells. Data are means ± SEM of four or five independent experiments, each with a different donor. $*P < 0.05$, $***P < 0.001$ by one-way ANOVA. (**B**) RT-qPCR analysis of *MMP1*, *MMP13*, and *MMP14* mRNA abundances in M-CSF-MDMs stimulated with LPS or FBG for 4 (*MMP13*) or 24 hours

Europe PMC Funders Author Manuscripts

(*MMP1* and *MMP14*) in the presence or absence of 3 μM TAK-242 or DMSO. Data are presented as the percentage change in mRNA abundance relative to that in cells stimulated with LPS or FBG in absence of TAK-242. Data are means ± SEM of three or four independent experiments, each with a different donor. **** $P < 0.0001$ by one-way ANOVA. (**C**) Collagen film degradation by M-CSF-MDMs stimulated with or without (−) LPS or FBG in the presence or absence of 10 μM GM6001 for 5 days. Digested areas of collagen are shown as white regions against a gray collagen background. Images are representative of three independent experiments, each with cells from a different donor. (**D**) Top two rows: Fluorescent gelatin film degradation by M-CSF-MDMs stimulated with or without (−) LPS or FBG in the presence or absence of 10 μM GM6001 for 64 hours. Digested areas of gelatin are shown as black regions against a green gelatin background. Bottom row: Cell surface MMP14 and DAPI (4′,6-diamidino-2-phenylindole) immunofluorescence staining are shown in red and blue, respectively. In this panel, “C” denotes cells stained in the absence of primary antibody. Third row: merged views of gelatin degradation and MMP14 immunofluorescence. Images are representative of three independent experiments, each with cells from a different donor. Scale bar, 18.00 μm.

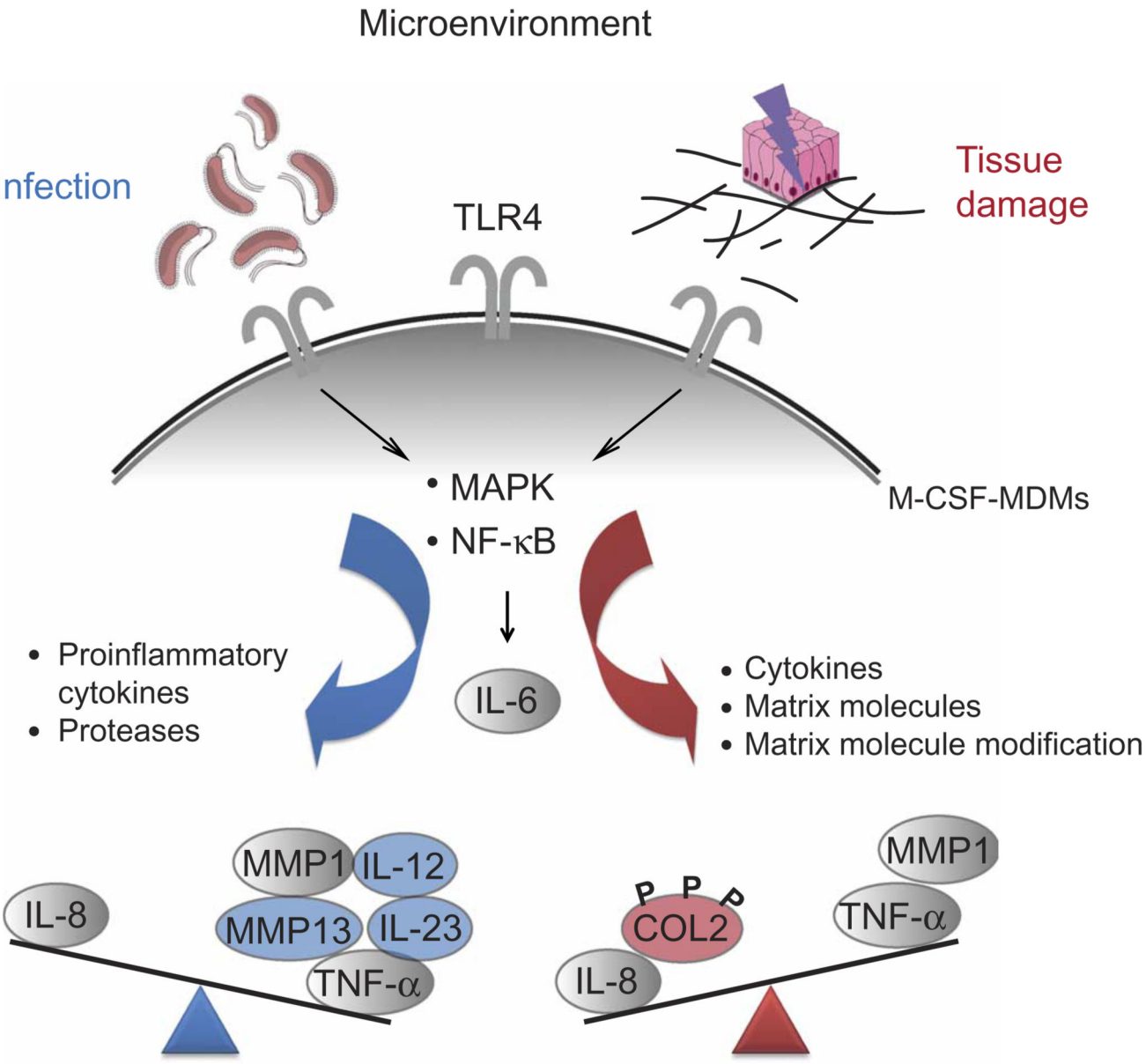

Fig. 7. Model of the microenvironmental influence on TLR4-mediated innate immune responses in macrophages.

TLR4 is exposed to and activated by ligands from distinct microenvironments, including infected as well as sterile, but damaged, tissues. Both stimuli equally lead to activation of the NF-κB and MAPK signaling pathways and secretion of IL-6. However, whereas infection results in macrophages producing large amounts of proinflammatory cytokines and tissue-degrading enzymes, tissue damage promotes the synthesis and posttranslational modification of matrix molecules in addition to contributing to cytokine synthesis. Molecules whose production is stimulated exclusively by pathogens or tissue damage are shown in blue or red, respectively; those induced by both stimuli are shown in gray. P, phosphorylation.